This is to certify that the

thesis entitled

A Comparison of Measurement to Simulation
for an Antenna on a Vehicle

presented by

Michael Robert Markey

has been accepted towards fulfillment
of the requirements for

M.S. degree in Electrical Engineering

Edward J. Rothwell
Major professor

Date 4-15-03

PLACE IN RETURN BOX to remove this checkout from your record.
TO AVOID FINES return on or before date due.
MAY BE RECALLED with earlier due date if requested.

DATE DUE	DATE DUE	DATE DUE

6/01 c:/CIRC/DateDue.p65-p.15

A COMPARISON OF MEASUREMENT TO SIMULATION FOR AN ANTENNA ON A VEHICLE

By

Michael Robert Markey

A THESIS

Submitted to
Michigan State University
in partial fulfillment of the requirements
for the degree of

MASTER OF SCIENCE

Depart of Electrical Engineering

2003

ABSTRACT

A COMPARISON OF MEASUREMENT TO SIMULATION FOR AN ANTENNA ON A VEHICLE

By

Michael Robert Markey

As consumers require a growing number of information and entertainment systems in an automobile, the number of antennas integrated into a vehicle increases. A first pass approach to development of these antennas can be done with simulation. As the antennas operate at higher frequencies, however, simulation can become computationally expensive since the vehicle itself is part of the antenna. The Method of Moments (MM) technique is applied for a variety of frequencies ranging from 70 MHz to 1 GHz. Incorporating the Physical Optics (PO) approximation in a hybrid MM-PO approach can reduce the required RAM. The accuracy of the simulation results also needs to be verified with measurement. The measurements are performed at an advanced facility that allows a full three-dimensional radiation pattern measurement. These measurement and simulation results are compared.

For my parents

ACKNOWLEDGEMENTS

I would like to thank Dr. Rainer Kronberger for his enthusiastic support for this research. Thanks Rainer for arranging for me to come to Germany for this research. Your continued interest in the results of this study has been inspirational to me. Thanks again for coming all the way to East Lansing for the defense.

Thanks to the whole EAA group at FUBA® Advanced Reception Systems in Bad Salzdetfurth, Germany. Thanks especially to Axel Stephan for your patience and experience with measurements and your helpful advice with simulation.

Thanks to Dr. Leo Kempel and Dr. Ed Rothwell for your wisdom and guidance for this project and throughout my academic career. Go Green!

TABLE OF CONTENTS

LIST OF TABLES

LIST OF FIGURES

Images in this thesis are presented in color.

CHAPTER 1

INTRODUCTION

1.1 Overview

Consumers are increasingly demanding multimedia applications for their automobiles. They are also considering the availability of information and communications systems when purchasing a vehicle. The growth in demand for these systems means that the information flow between the vehicle and various sources is of increasing importance. This has lead to a variety of antennas needed on the vehicle to allow communication with terrestrial and satellite sources. As illustrated in Figure 1.1 [1], a current automobile could have numerous antennas to handle services such as AM/FM radio, television, mobile phone, satellite digital audio radio (SDARS), global positioning satellite (GPS) system, remote keyless entry (RKE), radar systems and several others. In the near future, vehicles could be equipped with Internet access and be Bluetooth compatible to allow wireless communications with computers, personal device assistants (PDA) and other computer and electronic equipment.

These several antennas pose a significant design challenge to engineers aiming to optimize each antenna to meet performance specifications. Unfortunately, the vehicle itself often has a large impact on performance since it is part of the antenna. This requires prototypes of the vehicles and expensive measurement time to determine how to optimally place the antennas. As design cycle times are reduced, however, prototypes are becoming more difficult to obtain and measurement time is even more precious. This has lead automotive antenna engineers to seek another means for design. Simulation, as a first pass approach to design, is a viable means to make some initial design decisions. Simulating the performance of an antenna with an automobile requires significant computational resources especially for high frequencies. Previous work [1] has shown that a method of moments simulation for the FM band ranging from 76-108 MHz on a vehicle compares very well with actual three dimensional pattern measurements. Many applications shown in Figure 1.1 require much higher operating frequencies. These higher frequency simulations may be too computationally expensive for a full method of moments simulation. Therefore, hybrid methods of simulation need to be explored to reduce the computational expense required for higher frequencies up to 1 GHz. These hybrid methods need to be compared with measurement to verify accuracy for a variety of bands of frequencies. These include Band FM (70-120 MHz), Band 3 (175-235 MHz), Band Own (250-450 MHz), Band 4-5 (670-870 MHz) and Band GSM (800-1000 MHz).

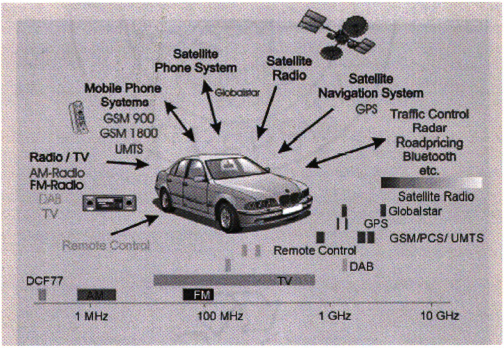

Figure 1.1: The many required communications with a vehicle. From [1]

1.2 Test Vehicle

To compare the hybrid methods of simulation with measurement, a model of a vehicle has been constructed. The model, or "test vehicle," is constructed in an attempt to make a realistically sized vehicle that is easy to create in simulation. For this reason, large, simple geometries and sharp corners are used instead of smooth curves that may be difficult to create virtually. Additionally, the test vehicle is simpler than the actual shell of a real vehicle because it does not contain complex materials and numerous discontinuities such as door hinges, seals and the vehicle interior. The test vehicle is constructed of wood and covered with brass mesh and conducting materials. It is 3.6 meters long, 1.6 meters wide and 1.56 meters tall. It is elevated from the ground by 0.44 meters. The test vehicle is pictured in Figure 1.2.

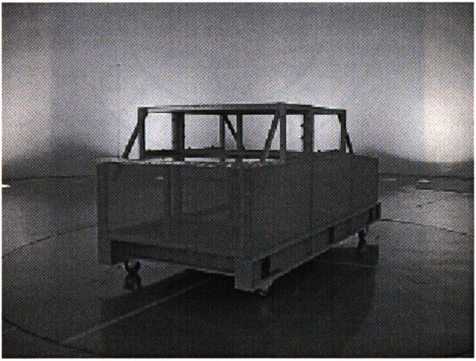

Figure 1.2: Simplified vehicle model constructed with wood and brass mesh

1.3 Measurement

In order to completely compare a simulation result with measurement, a full three-dimensional measurement must be taken. This is performed at the radome. The radome is a sophisticated range facility that allows a three-dimensional near field measurement. After the measurement is complete, the data is transformed to far field data that can be compared with simulation. A vehicle is shown in Figure 1.3 inside the radome. The large arm protruding upward is the elevation arm that suspends a broadcasting antenna at various elevation angles (θ). The vehicle containing the receiving test antenna is rotated on a turntable for various azimuth angles (ϕ). In this way, a full scan can be performed. The measurements are discussed in detail in Chapter 2.

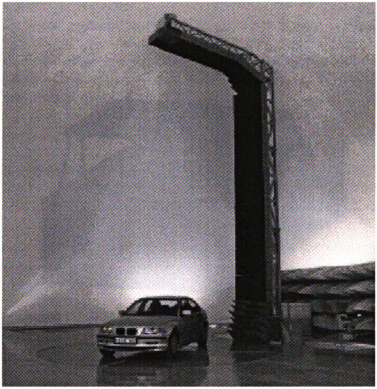

Figure 1.3: A typical near field scan on a vehicle inside the radome

1.4 Simulation

Since the aim of the study is to compare the measurements taken on the vehicle to simulations, a simulation model must also be constructed. The simulation model is shown in Figure 1.4 as constructed in FEKO. FEKO stands for "Field Computations Involving Objects of Arbitrary Shape." The simulation model has exactly the same dimensions as the physical test vehicle. It is covered with a triangular mesh to allow the application of the method of moments and other simulation techniques. The mesh sizing can be adjusted with frequency. The simulations are discussed in detail in Chapter 3. The comparison of results from measurement and simulation are shown in Chapter 4. Chapter 5 includes the conclusions to this study.

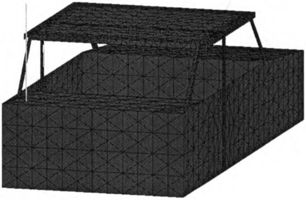

Figure 1.4: Simulation model of a vehicle

CHAPTER 2

DESCRIPTION OF MEASUREMENTS

2.1 Introduction to the Antenna Measurements

There are many different types of measurements to characterize the performance of an antenna on an automobile. The automotive industry has an increased interest in accurate high frequency measurements of many antenna performance parameters. This interest has been motivated by an increased consumer demand for automotive electronics that require communication with terrestrial and satellite antennas under harsh conditions. These electronics include communication and entertainment equipment that require ever increasing data transfer rates that operate at higher frequencies. This has led to significant design challenges for an effective antenna on the automobile. Measurements have been a key factor for assessing the performance of the design. Simulation may point to some new design solutions, decrease design time, and reduce overall design cost, but it is still necessary to take thorough measurements to verify the antenna design is within specifications.

The first step in typical high frequency antenna development for a vehicle is to design the antenna in free space without the vehicle. This is usually done for frequencies greater than 1 GHz. This design is often modeled using software. Once the simulated performance is within specification then the first prototype of the antenna is constructed. This prototype antenna is tested in an anechoic chamber and a comparison between the modeled performance and the actual measurements is made. The prototype then needs to be optimized or redesigned to correlate with simulation if necessary. After this phase, the antenna is actually mounted on a vehicle and measured. This is the final step in the initial development of a communications antenna for a vehicle [1]. It is this final step in the initial development of the antenna that will be discussed since the overall goal is to compare the measurement of the antenna on the vehicle to the simulation of the antenna on the vehicle.

The problem of how to take an accurate three dimensional antenna measurement on a vehicle has been faced by many automotive engineers. A simple method for taking a pattern measurement involves driving the test vehicle in circles around a broadcasting antenna. The irreproducibility of these measurements, in addition to the susceptibility to outdoor environmental conditions, does not allow for a good means of measurement [1]. Furthermore, this measurement technique does not capture a three-dimensional pattern measurement that is necessary to meet specification for many applications, including satellite communications.

The use of a sophisticated range facility leads to more accurate results that are fast and reproducible. A radome that encloses the vehicle, antenna, and measuring equipment for the purpose of weather protection is one such facility. The radome allows far field measurements to be taken by rotating the vehicle on a turntable. Almost full three-dimensional measurements can also be taken by a scanning near field antenna system enclosed in the radome. The near field measurements can then be transformed to far field radiation patterns [2]. When the near field measurement antenna is stored below the conducting ground, an accurate impedance measurement of the antenna mounted on the vehicle can also be made. Despite the flaws, which every range facility has, the radome provides a good means for taking a combination of measurements.

With this facility, advances in the use of simulation are possible since there is a means of accurately benchmarking the antenna simulation performance. The measurements taken for this investigation are done such that exactly the same test can be simulated with the software package FEKO [3], which is the basis for this investigation. The input impedance, far field radiation pattern and near field scan measurements will be discussed in the following sections.

2.2 The Input Impedance Measurement

The measurement of input impedance of the antenna on the vehicle is very important. The antenna input impedance should be closely matched for all desired frequencies. For this study, the frequencies range from 70 MHz to 1 GHz. Since this is such a large range, the frequencies are divided into five smaller bands. These bands include the FM band defined here as beginning at 70 MHz and spanning to 120 MHz. Band 3 spans from 175 MHz to 235 MHz. Band "Own" spans from 250 MHz to 450 MHz. Band 4-5 begins at 470 MHz and ends at 870 MHz and finally Band GSM begins at 800 MHz and ends at 1 GHz. There are some spaces between the bands where certain frequencies are not tested.

Since a monopole antenna is easily obtainable but has a relatively small bandwidth, a reference monopole antenna for each band is used. The system uses a characteristic impedance of 50 Ohms. The ideal impedance of a monopole is 36 Ohms, which is near 50 Ohms. Thus, the input impedance should be nearly matched to 50 Ohms for each tested antenna. For this reason a quarter wavelength monopole is the chosen test antenna, and a different antenna is cut for the center frequency of each band. The preliminary lengths of the monopoles are cut to $\lambda/4$ since the input impedance of a quarter wavelength monopole on an infinite ground plane is fairly well matched to 50 Ohms. Further trimming the monopoles to the proper lengths achieves a better match for the center frequency for each of the bands as determined by using the vector network analyzer. Once all the test antennas are matched at the center frequencies of the different bands, the input impedance is ready to be measured for each band.

To do this, the vehicle is situated on the center of the turntable in the radome. The elevation arm, which is used for near field measurements, is stored below the conducting ground to prevent the vehicle antenna from having any mutual impedance due to coupling with the arm. The network analyzer is then calibrated to the feeding point on the vehicle to account for additional cable that causes loss and electrical delay. The input impedance measurements are then performed throughout the frequency ranges for each monopole mounted on the test vehicle. This measurement takes a very short time since there are no movements of the vehicle or measuring equipment. The time to take the measurement is determined only by the network analyzer and is usually done in less than a second as the analyzer sweeps the desired frequencies. Table 2.1 shows a list of the tested frequencies with their center frequency and the length of the quarter wavelength monopole that gives the best match on the network analyzer. The results are shown on a smith chart for clarity. Figure 2.1 (a) includes the input impedance for the FM band and (b) for Band 3. Figure 2.2 (a) includes an input impedance plot for Band Own and (b) for Band 4-5 and finally Figure 2.3 illustrates the resulting input impedance for Band GSM. Notice the center of the curve passes through the center of the smith chart due to the monopole being matched for the center frequency of each band. The input impedance is an important parameter of an antenna and good measurements are needed to make a careful comparison to the simulation.

Band	**Start Frequency (MHz)**	**Center Frequency Used (MHz)**	**Stop Frequency (MHz)**	**Monopole Length (cm)**
FM	70	90	120	85
3	175	205	235	36
Own	250	350	450	21
4-5	470	670	870	11
GSM	800	900	1000	8.5

Table 2.1: The lengths of monopoles used for each band

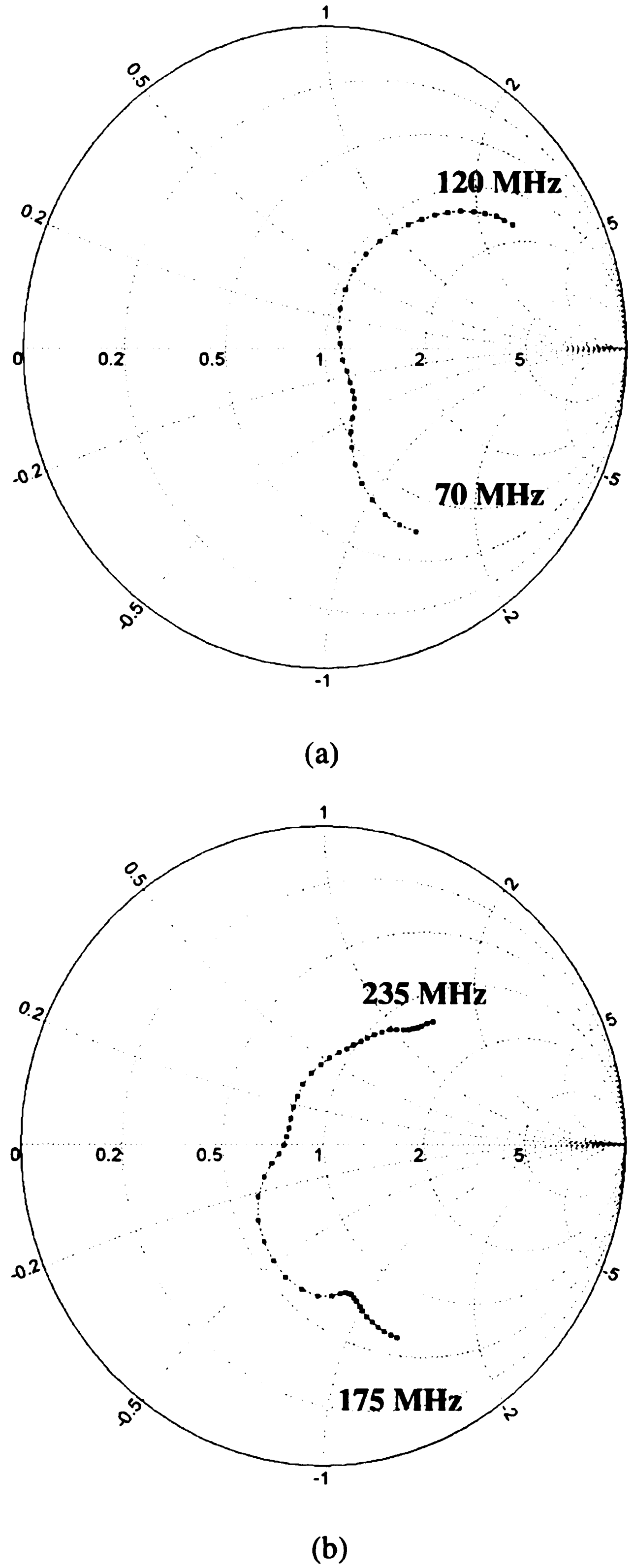

Figure 2.1: Input impedance on a standard Smith Chart for (a) Band FM 70-120 MHz and (b) Band 3 175-235 MHz

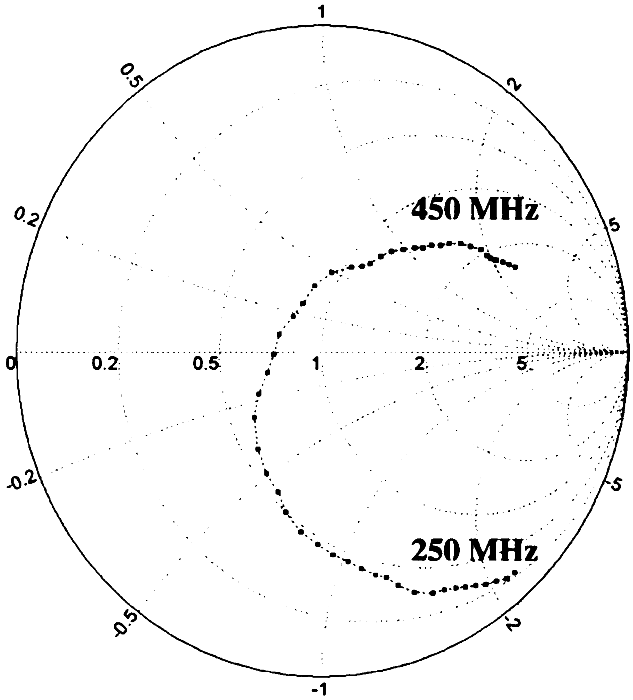

(a)

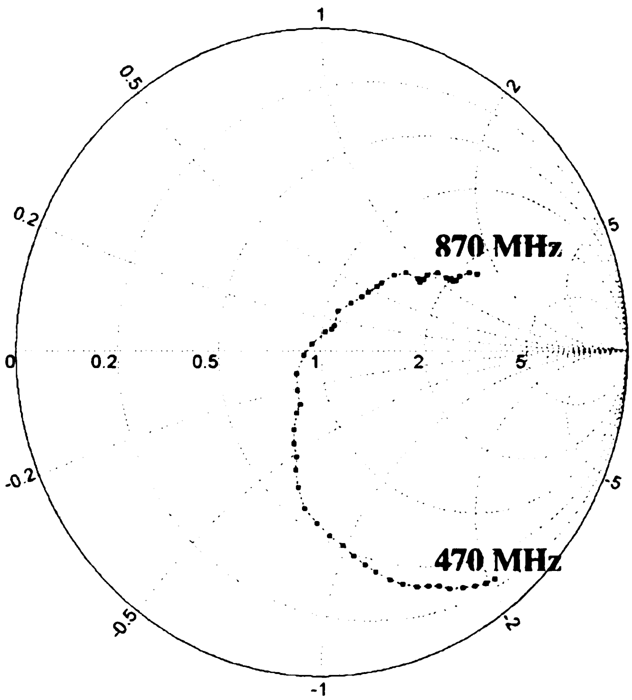

(b)

Figure 2.2: Input impedance on a standard Smith Chart for (a) Band Own 250-450 MHz and (b) Band 4-5 470-870 MHz

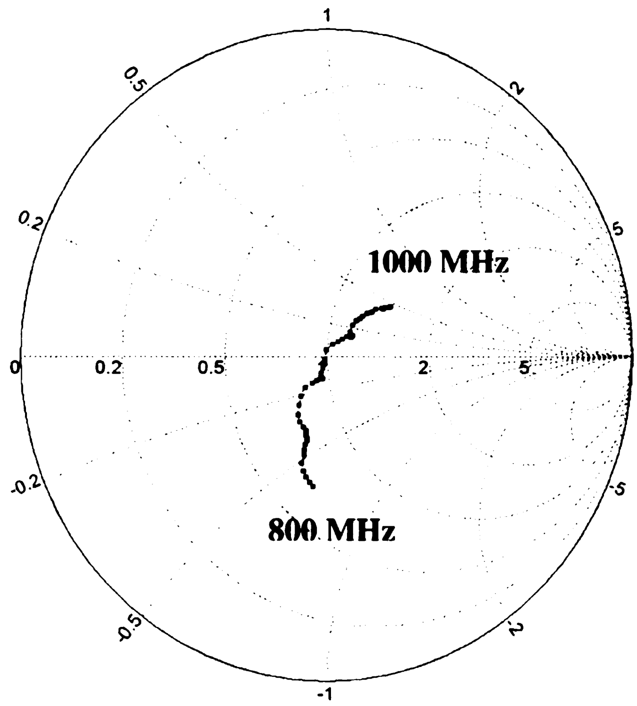

Figure 2.3: Input impedance on a standard Smith Chart for Band GSM 800-1000 MHz

2.3 Far Field Measurements

The far field radiation pattern is a crucial performance characteristic of an antenna. Since it is so descriptive of antenna behavior, a far field radiation pattern is often given in some manner as a design specification. The measured far field radiation pattern is important for this study to verify the accuracy of the far field data that is extracted from the near field data. It is also useful to see an additional accurate low elevation angle measurement. The far field measurements are also vital for comparison with simulation since FEKO computes the far field radiation pattern for the vehicle.

The far field radiation patterns are taken with the center of the vehicle situated at the center of the turntable. The turntable is housed within a weather-protecting radome. The radome's hemispherical shell of material allows electromagnetic waves to propagate through with small attenuation and little dispersion for many frequencies of interest. The outdoor far field antenna is situated 100 meters from the center of the radome. The far field region begins at $d_{farfield} = \frac{2 \cdot D^2}{\lambda}$, where D is the maximum dimension of the antenna and λ is the wavelength in free space. The largest dimension D of the test vehicle is the length of the vehicle (3.6 m). The far field region should also be at least 10λ due to the phase error of 23° that is a result of the non-planar wave front. This means that the far field region ranges from $10\lambda \approx 42$ meters for 70 MHz and 86.40 meters for 1 GHz. This is well into the far field region since the test frequencies explored are within the range of 70 MHz to 1 GHz. The far field antenna is separated from the vehicle by a distance of roughly 23λ for 70 MHz and about 333λ

for 1 GHz. The outdoor far field antenna is log-periodic and is designed for all tested frequencies. This outdoor antenna transmits and the vehicle antenna receives after the wave passes through the radome. The geometry for this measurement setup is illustrated in Figure 2.4.

A control room beneath the radome sends a transmitting signal to the far field antenna using a computer and the vector network analyzer. The vector network analyzer used for all measurements is an HP 8753 ES. The outdoor antenna transmits and a short while later the device under test (DUT) receives the transmission. The computer records the received signal strength as measured by the network analyzer and controls the turntable to rotate a specified angle. It repeats the transmission, reception and recording process for the entire 360-degree range. It is important to align the vehicle on the turntable properly to ensure correct measurements for all angles.

After a given measurement is taken the control room can rotate the outdoor log periodic antenna to take a different polarization measurement. The measurement process is the same for both polarizations except that the outdoor antenna is oriented vertically for one polarization measurement and horizontally for the other. This allows the measurements of far field vertical (FFV) and far field horizontal (FFH) polarization radiation patterns. Note that this measurement gives the radiation pattern for only one elevation angle $\theta \approx 85°$ but all rotational angles ϕ taken as specified by the controlling computer. Therefore, this measurement alone cannot be used to verify a simulated radiation pattern but can be useful in verifying one cut.

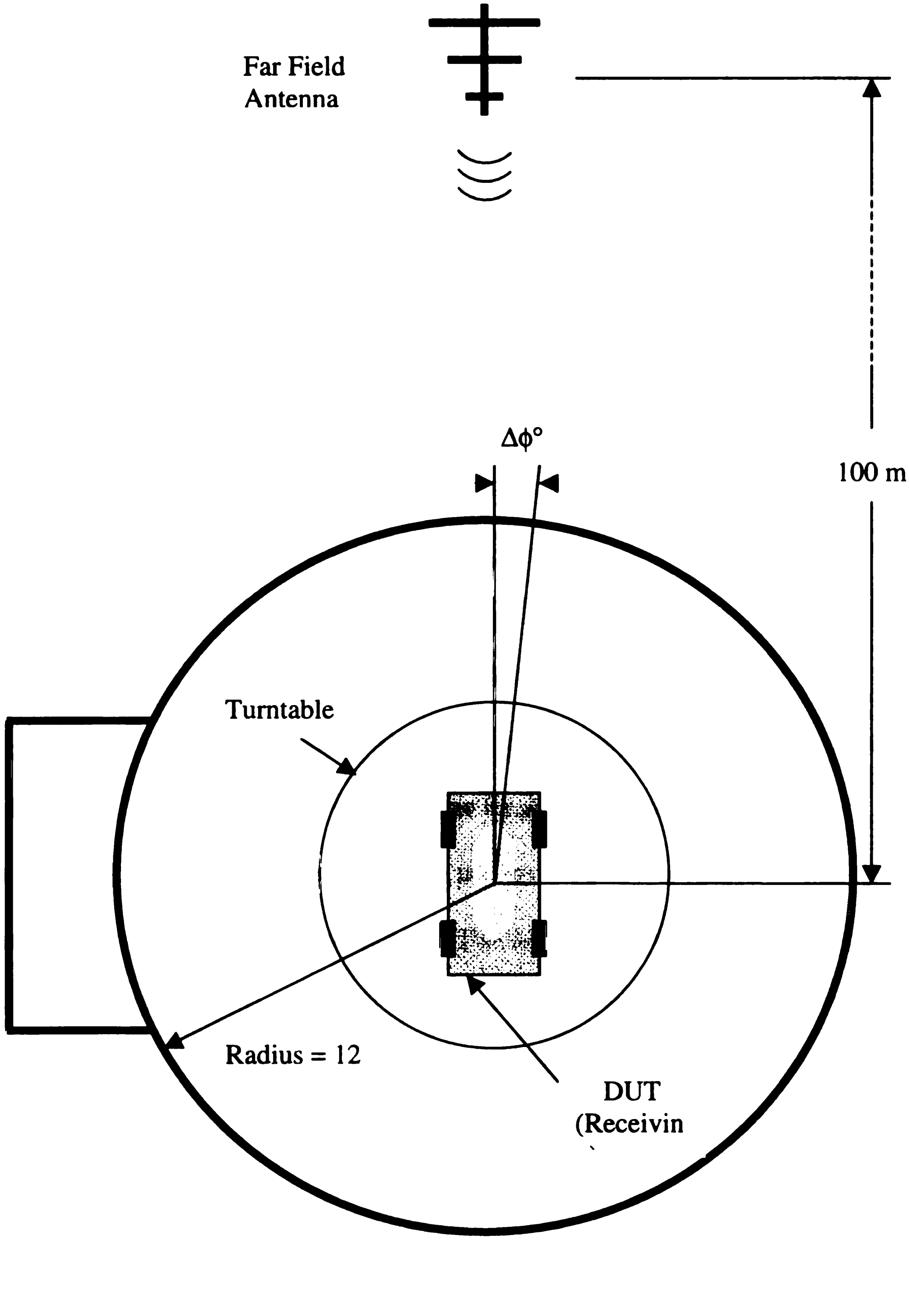

Figure 2.4: The Radome setup for the far field measurement

As mentioned above, the control room rotates the turntable a certain angle between measurements. This rotational or azimuth resolution angle $\Delta\phi$ is chosen to be 2.5°. This requires 144 measurement points over the rotation of the turntable. A finer resolution could be used at the radome facility (about 0.1° minimal). However, a 2.5° resolution is used to allow an easy comparison with simulation and also with far field data transformed from near field data which both use a 2.5° resolution. The elevation angle of the far field antenna has been determined experimentally to be near 85°. This can be seen by comparing the transformed near field to far field data to that of the actual far field data. This can be seen in several comparisons of far field measurements with transformed near field measurements.

The far field measurements are taken for all previously described bands. For each frequency band the corresponding monopole antenna is attached to the top of the rear left trunk. The measurement times for the far field scan are very small. The turntable that controls the azimuth direction ϕ turns at a rate that allows all 144 measurements to be taken in a few minutes. This time is independent of the frequency band, but dependent on the bandwidth. If a larger bandwidth is required then the turntable automatically adjusts the angular velocity resulting in slightly longer measurement time. The results for these measurements are shown graphically for the center frequency of Band FM (92 MHz) in Figures 2.5 and 2.6. Figure 2.5 shows the FFV pattern of the vehicle in normalized dB. The front of the vehicle is aligned with 0° and a maximum in the radiation pattern is normalized to 0 dB. Figure 2.6 illustrates the normalized FFH pattern of the vehicle in dB. Figures 2.7 and 2.8 show Band 3 normalized FFV and FFH respectively for the center frequency of 205 MHz. Figures

2.9 and 2.10 show Band Own normalized FFV and FFH respectively for the center frequency of 350 MHz. Figures 2.11 and 2.12 show Band 4-5 normalized FFV and FFH respectively for the center frequency of 670 MHz. Figures 2.13 and 2.14 show GSM normalized FFV and FFH respectively for the center frequency of 900 MHz. The rectangular shape in the center of these plots is representative of the vehicle with the front facing 0°. These results will be used later in the comparison of radiation patterns to those of simulation.

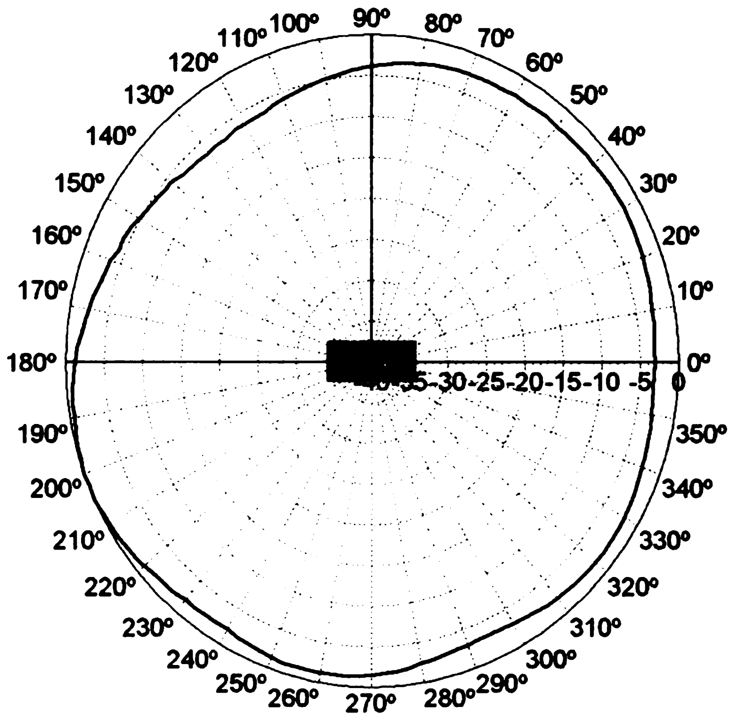

Figure 2.5: 92 MHz Band FM Far Field Vertical (Normalized Amplitude dB)

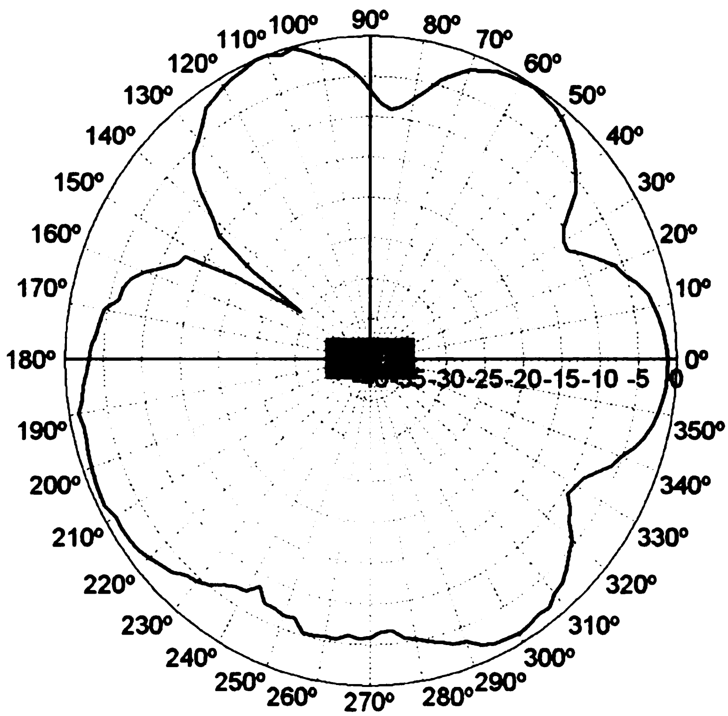

Figure 2.6: 92 MHz Band FM Far Field Horizontal (Normalized Amplitude dB)

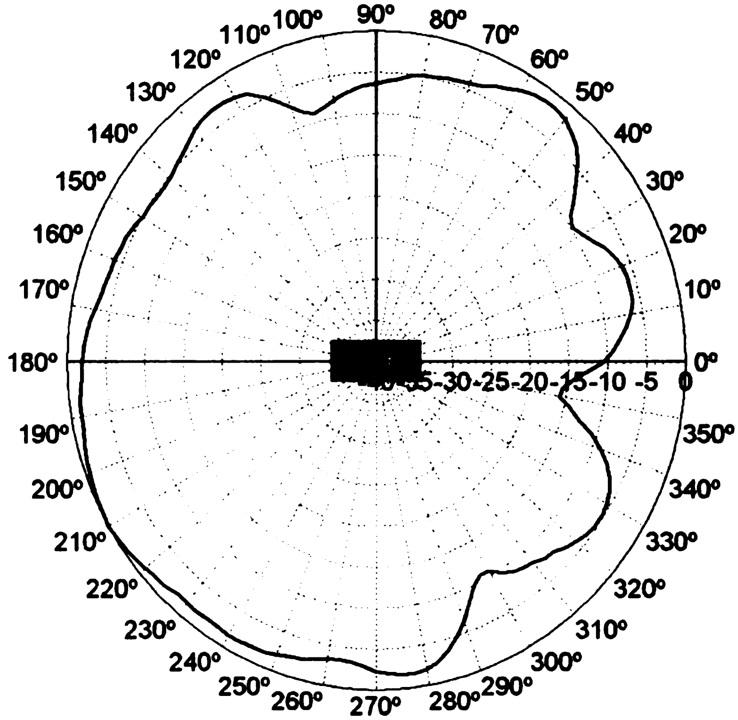

Figure 2.7: 205 MHz Band 3 Far Field Vertical (Normalized Amplitude dB)

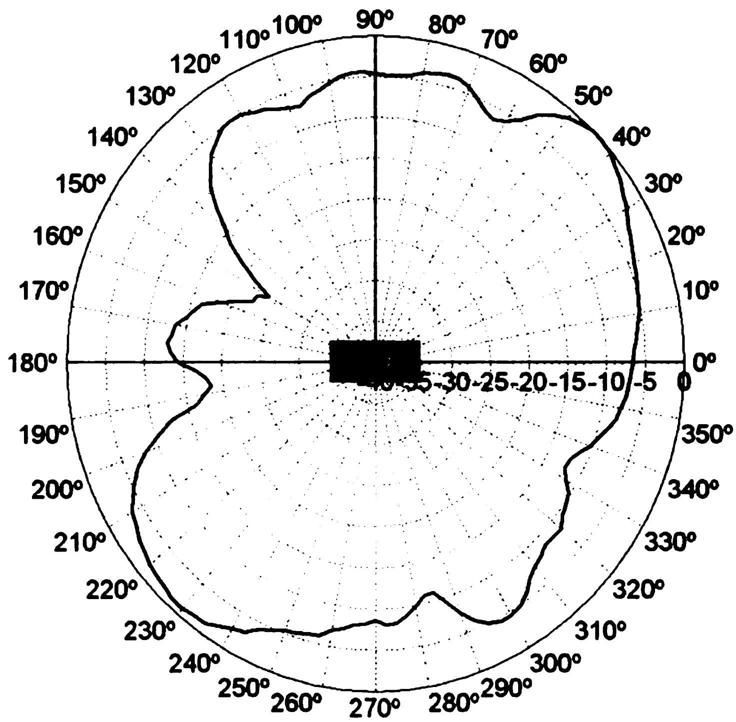

Figure 2.8: 205 MHz Band 3 Far Field Horizontal (Normalized Amplitude dB)

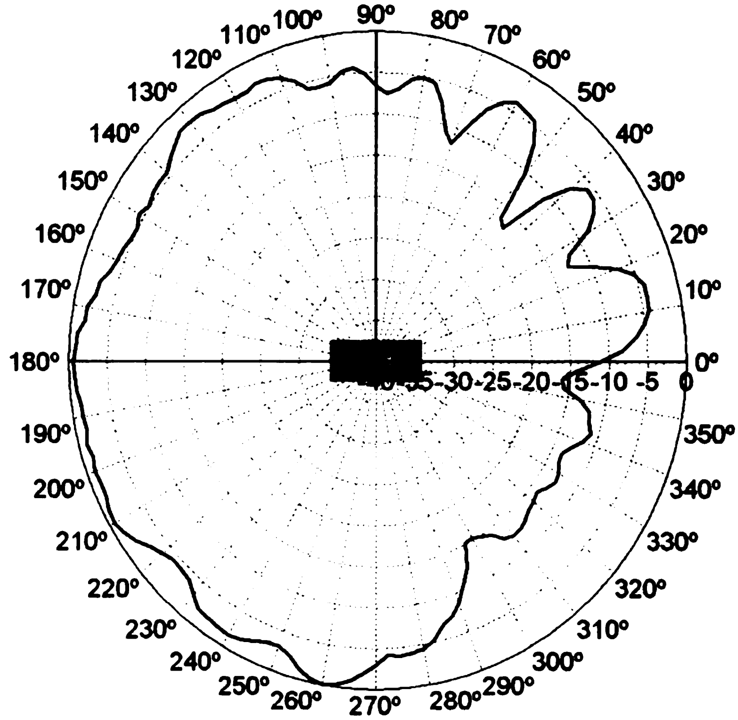

Figure 2.9: 350 MHz Band Own Far Field Vertical (Normalized Amplitude dB)

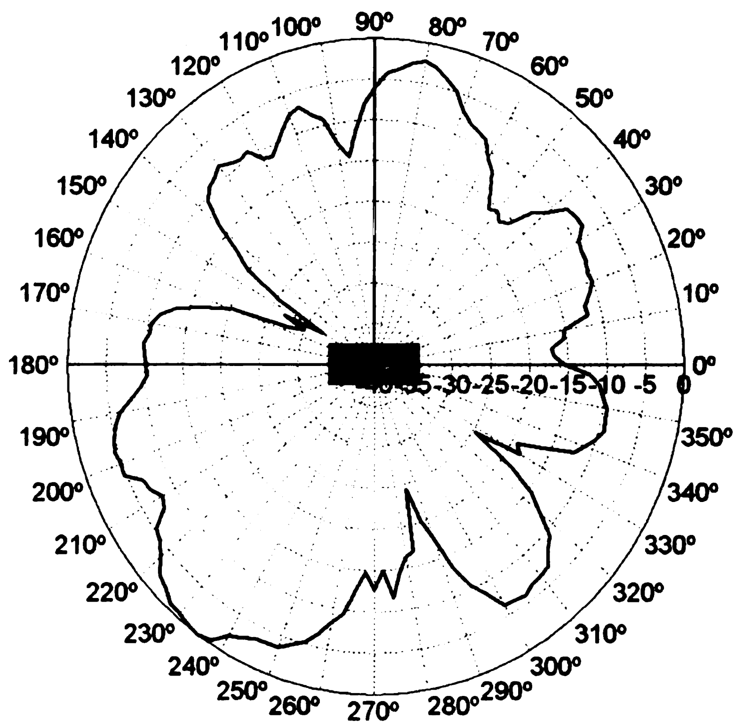

Figure 2.10: 350 MHz Band Own Far Field Horizontal (Normalized Amplitude dB)

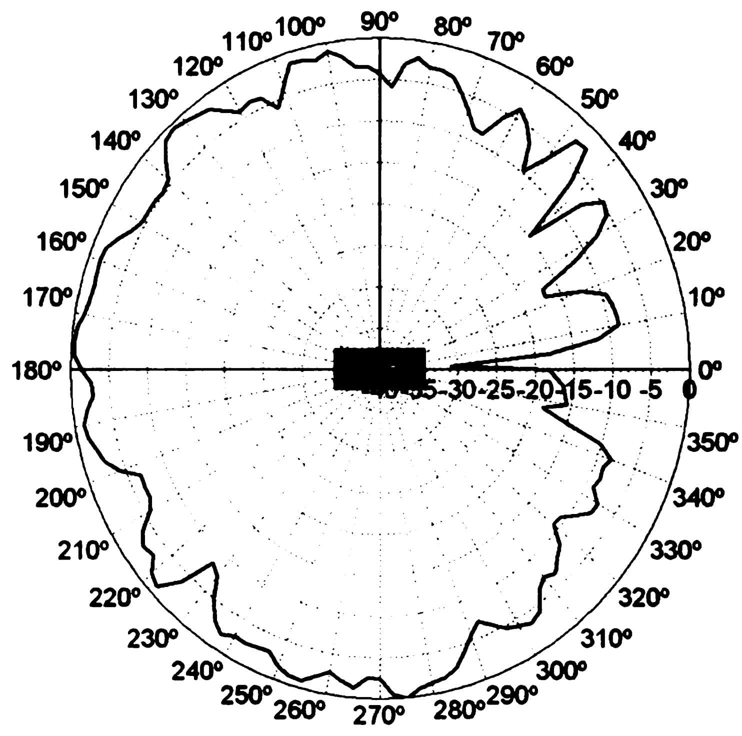

Figure 2.11: 670 MHz Band 4-5 Far Field Vertical (Normalized Amplitude dB)

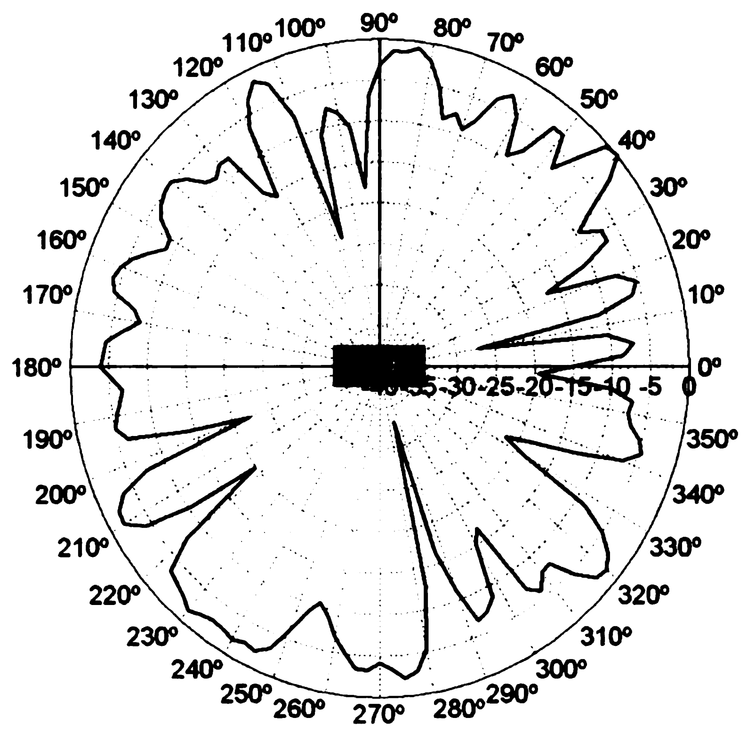

Figure 2.12: 670 MHz Band 4-5Far Field Horizontal (Normalized Amplitude dB)

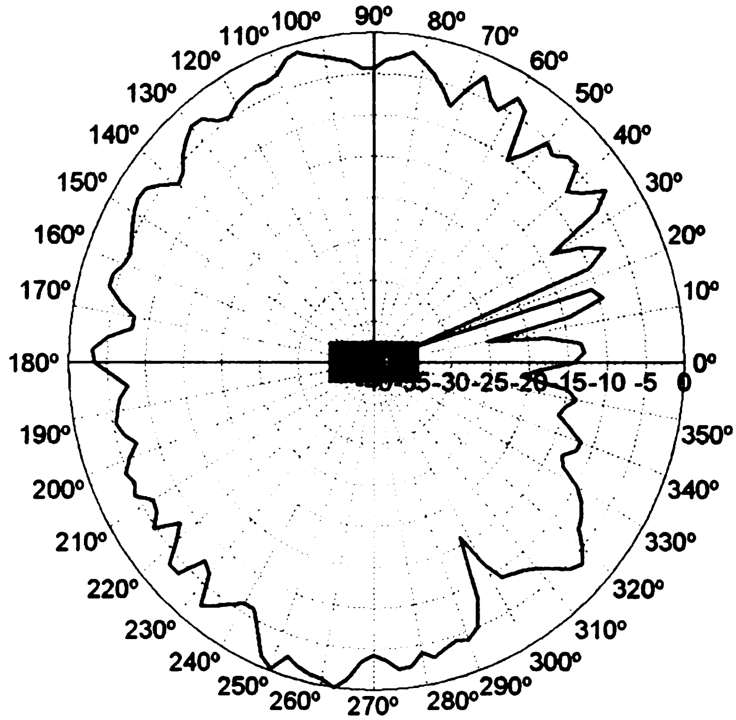

Figure 2.13: 900 MHz Band GSM Far Field Vertical (Normalized Amplitude dB)

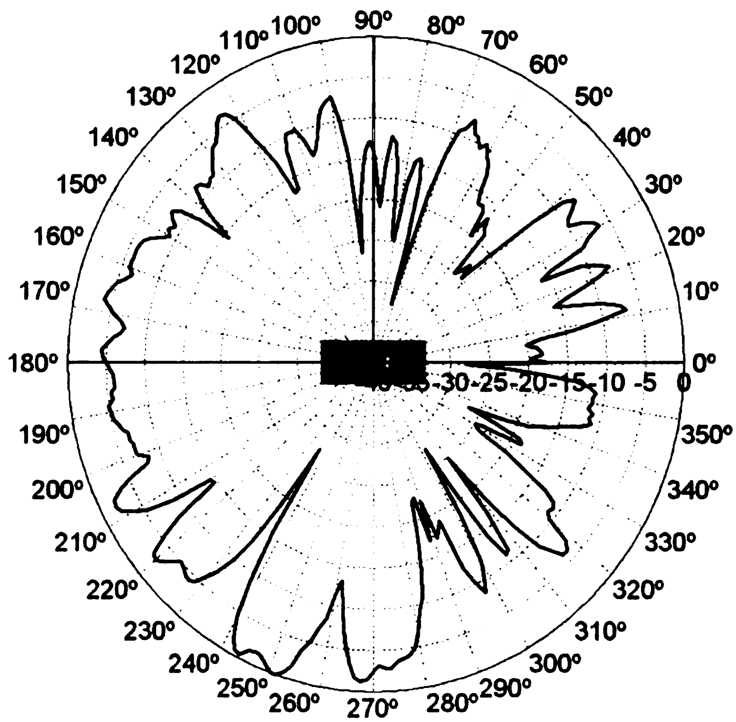

Figure 2.14: 900 MHz Band GSM Far Field Horizontal (Normalized Amplitude dB)

2.4 Near Field Measurements

The near field measurement is the most important quantity for making a comparison to simulated results from FEKO. The near field scan enables a full three-dimensional far field radiation pattern to be observed through the use of transformations. These transformations are performed after the near field measurement is complete by software that is associated with the measurement facility. A brief presentation of the basic near field theory is discussed followed by the measurement procedure and some typical results.

Near field scanning technology has been explored in some fashion as early as the 1950's [4]. The method of scanning the near field is based on scanning over a known three-dimensional geometry very close to the antenna. Typical scanning geometries include a plane, cylinder or sphere. While there are some advantages to using a planar or cylindrical scanning geometry, the spherical system is used in many cases since it allows the most complete calculation of the far field radiation pattern [5]. An antenna on an automobile needs an accurate predication of the far field for all angles whereas a horn antenna, for example, needs only some angles to be predicted. It is therefore necessary in this study to scan over a spherical geometry to achieve the most accurate prediction for all angles. The spherical transformation is generally the most mathematically complicated and requires the most computation time [6]. With modern computers, however, this is performed easily for most frequencies. Measuring the magnitude and phase over this minimum geometry at the proper resolution and at two orthogonal field components E_ϕ and E_θ allows for a modal transformation to a full far field three-dimensional pattern.

A problem facing the near field measurement is that there is a radiation pattern associated with the transmitting test antenna in addition to the DUT. This means for some elevation and azimuth angles, low signal strength could be measured where there is in fact simply a null in the probe's radiation pattern. This is overcome by using probe compensation. Probe compensation is based on spherical wave modal expansion. A spherical wave can be decomposed to represent a superposition of spherical waves, all monochromatic, traveling in different directions with different amplitudes. The expansion determines the unknown amplitudes and directions of these propagating waves through the use of superposition. The probe output is determined as a function of these expanded fields. The result is a relationship between the known field-pattern of the probe to the unknown field associated with the DUT [2]. This relationship is specified by the use of spherical mode coefficients for the probe antenna contained in the software used to extract the far field data. A correction is made to the pattern and polarization due to the characteristics of the transmitting probe antenna.

The radome facility achieves a spherical scanning geometry by mounting the probe antenna on an elevation arm that is 10 m long. It rotates this probe antenna around the DUT at a constant radius of 10 m for various angles of θ by moving the elevation arm. The arm is referred to as an elevation arm since it changes only the elevation angle; the turntable is needed to change the azimuth angle. Using the turntable and elevation arm a semispherical geometry can be scanned for nearly all angles. If the sphere is sampled at a resolution of $\Delta\theta = \frac{1}{2} \cdot \frac{\lambda}{(b+\lambda)}$ and

$\Delta\phi = \frac{1}{2} \cdot \frac{\lambda}{(b+\lambda)}$ then the radiation characteristics of the DUT are fully extracted in the transformation [5]. The smallest wavelength of the tested frequency is denoted as λ and b is the radius of the smallest sphere that encloses the body of the vehicle. For the test vehicle used this is b = 2 m. Note that $\Delta\theta = \Delta\phi$ and that taking additional data points at a smaller resolution does not, by the Nyquist sampling theorem, increase the accuracy of the transformation.

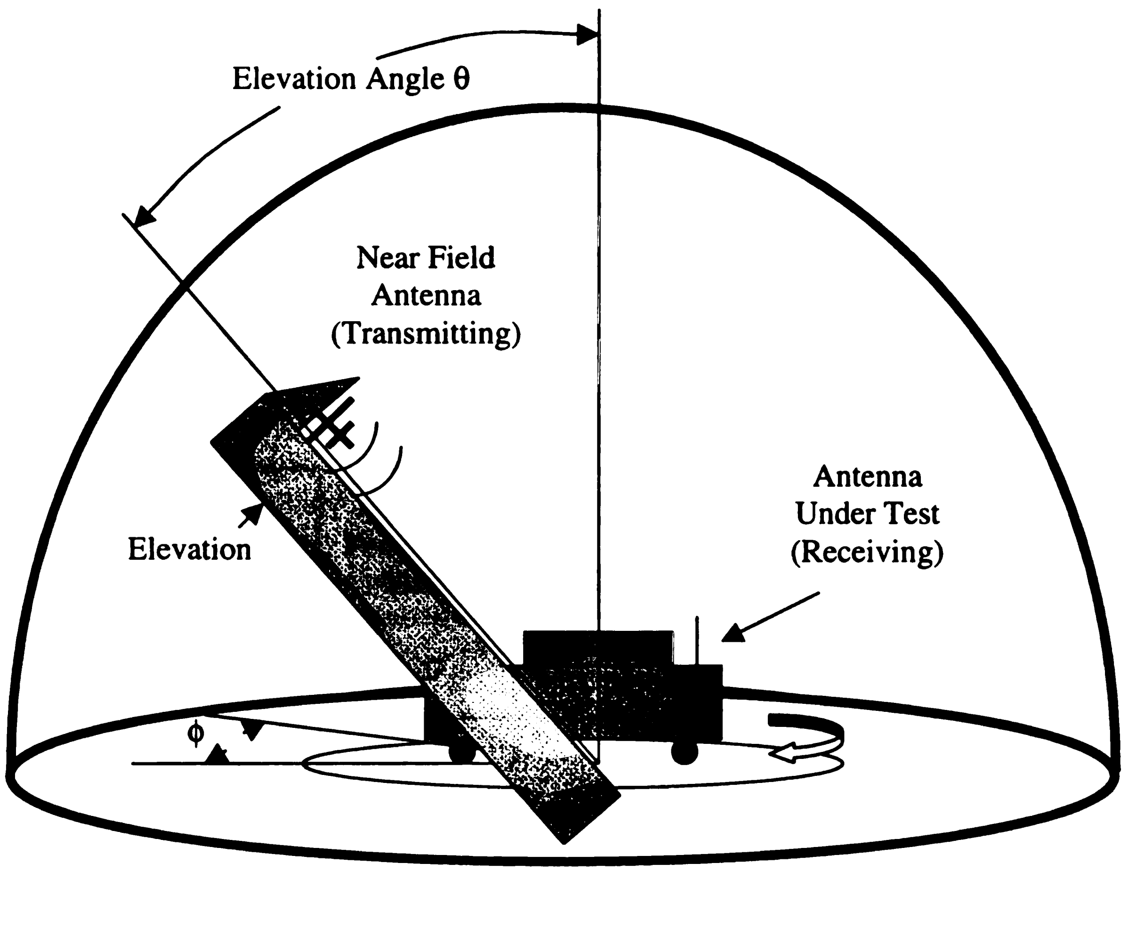

Figure 2.15: Illustration of the near field measurement

This measurement is taken in the radome with the elevation arm as mentioned above. The setup is illustrated in Figure 2.15 with the vehicle situated in the center of the turntable. The elevation arm hoists the near field antenna to the correct elevation angle θ and then the turntable is rotated for a changing azimuth ϕ. The elevation arm can illuminate the vehicle for all elevation angles between $\theta = 0°$ (towards zenith) and $\theta = 88°$ (near the ground). The probe antenna transmits and the vehicle on the turntable receives the signal. The elevation arm is then rotated to a new elevation angle θ and the process repeats. The polarization of the near field antenna is then changed automatically and again the turntable is rotated while the measurements are performed. The change in polarization is necessary to capture E_ϕ and E_θ over the minimum sphere. This order of taking measurements is optimized for the time of measurement since the number of data points required is related to the test frequencies and the measurement times can be lengthy. See Table 2.2 for the near field scan measurement times for all tested bands.

Band	**Start Frequency MHz**	**Stop Frequency MHz**	**Number of ϕ Points**	**Number of θ Points**	**Total Measurement Time (minutes)**
FM	70	120	45	11	25
3	175	235	45	11	25
Own	250	450	120	28	90
4-5	470	870	120	30	100
GSM	800	1000	120	30	100

Table 2.2: The total time for a near field measurement

Some resolutions for $\Delta\theta$ and $\Delta\phi$ shown in Table 2.2 are smaller than they need to be. This is done to try and make the measurement consistent and simple. For example, the necessary resolution for band GSM is about 3.7° and 4.2° for Band 4-5. However, a $\Delta\theta = 3°$ resolution is used for both GSM and Band 4-5 so that the last elevation measurement taken would be at the greatest possible angle of 87°. This requires 29 points and is as close to 88° as possible. This forced the resolution of the azimuth $\Delta\phi$ to also equal 3°. This is a very convenient number since 3° divides evenly into 360° requiring 120 data points exactly. Though this resolution is unnecessarily fine for both Band GSM and Band 4-5, it maximizes the measured elevation range and therefore allows for the best transformation.

The probe antenna for lower frequencies, i.e. the FM band, is a large log periodic antenna. This large antenna does not allow the elevation arm to scan at very low elevation angles (near 88°) since the antenna itself would come in contact with the ground when the polarization is changed to vertical-polarization. For higher frequencies, i.e. Band 4-5, a smaller log periodic antenna is used in which case the arm can be lowered to greater elevation angles (up to 88°) without the probe antenna coming in contact with the ground. The problem with the larger antenna, however, does not cause major inaccuracies in the extracted far field data in most cases. This is because the scan resolution is determined by the maximum test frequency (minimum wavelength) and for lower bands the higher elevation angle measurements are not typically needed anyway. In the case that these measurements are needed for a transformation, the software has the option to fill any incomplete measurement data with zeros or, if preferred, with the data taken at the greatest assessable elevation angle. Filling the data with zeroes or the last available data can obviously affect the accuracy of the transformation and will be discussed later. This measurement data is then transformed to far field data with the use of the software. The transformation requires the proper discretization in the data points as stated above. The program also incorporates probe compensation from a file containing the spherical mode coefficients for the near field scanning antenna. Some far field patterns extracted from near field data are included below to give some examples of typical results. The data has been extracted to achieve a resolution of 2.5° for θ and ϕ. Clearly this amounts to too many cuts to be displayed here. Figure 2.16 (top), for example, shows the radiation pattern for 350 MHz with theta polarization taken at phi = 0°. Figure 2.16 (bottom) includes the radiation pattern for 670 MHz with phi polarization taken with the vehicle rotated 90°. The vehicle is shown in gray in the center of the radiation pattern in Figure 2.16. These are just sample cuts and will be used to make comparisons later to the simulated results.

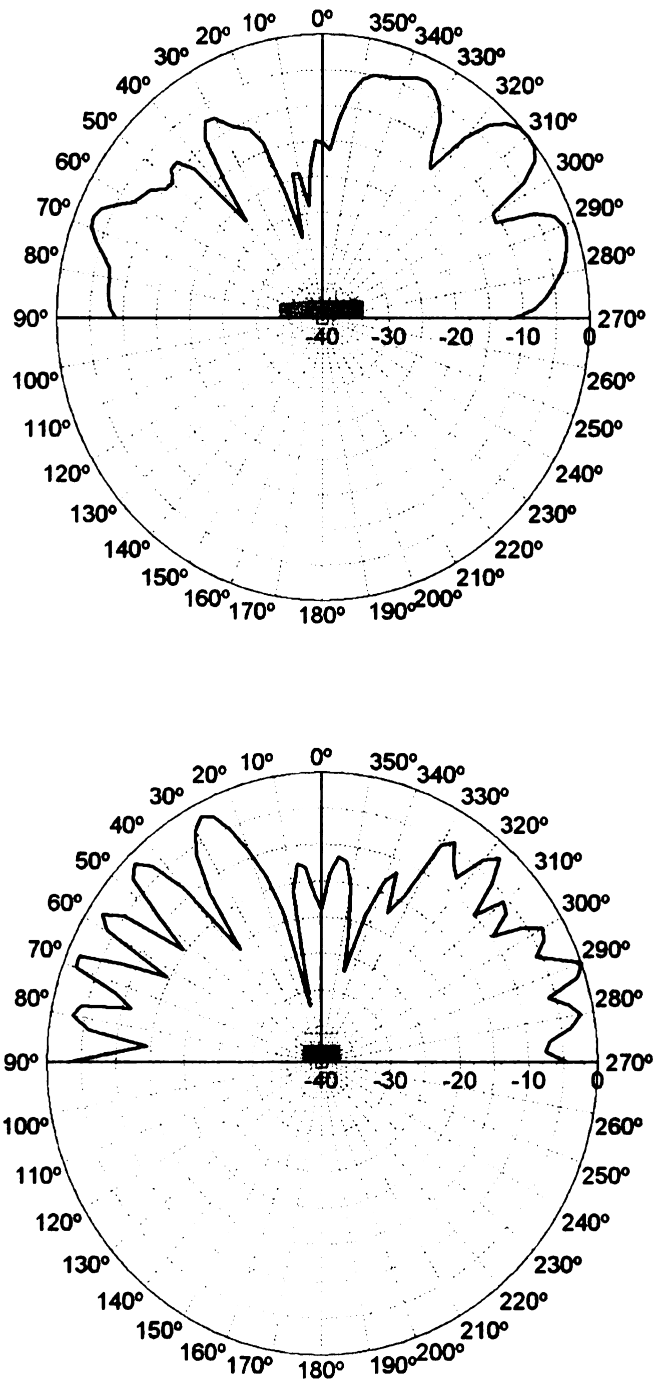

Figure 2.16: Illustrates the transformed radiation pattern for (top) 350 MHz for theta polarization with phi = 0° and (bottom) 670 MHz phi polarization with phi = 90° (Normalized Amplitude dB)

CHAPTER 3

SIMULATION METHODS

3.1 Introduction to Simulation Methods

As a vehicle begins to require a larger number of antennas at different frequencies for a variety of applications, simulation becomes a sensible means to verify the antennas are within their performance specifications. For antennas operating at higher frequencies, the placement of the antenna on the vehicle may be critical to its functionality. Additionally, antennas mounted on a vehicle perform quite differently than in free space. As designers look to lower design costs and cycle time, simulation becomes a viable approach for predicting this performance and determining the proper placement.

In most automotive scenarios, the performance of an antenna needs to be analyzed with the antenna in close proximity to other electrical bodies. In this study, for instance, an antenna is mounted on a vehicle that has sharp edges, pillars and other distinct regions. The vehicle geometry itself has a significant impact on the overall performance of the antenna. Since the vehicle plays such an active role in the radiating system, the vehicle geometry needs to be carefully considered in simulation to ensure an accurate solution for the characteristics of the antenna.

There are several different techniques used in computational electromagnetics to find this solution. A few of these techniques include the Method of Moments (MM), Physical Optics (PO) and the Uniform Theory of Diffraction (UTD). Each method has its own advantages and practical applications while also having unique drawbacks. Choosing the correct method to find the solution is important to help ensure computational errors and approximations will be reasonable and controlled. The type of problem, the available computational resources, and the difficulty of formulating a computer program to find the answer, all govern the best choice of technique.

The MM analysis is a well-known and fairly reliable means of characterizing the performance of an antenna for lower frequencies. This approach is often used as a reference for comparing other simulation results from different techniques. Many antenna geometries are conducive to using the Method of Moments [16]. The method of moments can be applied to complex geometries where electrical bodies are in close proximity to the antenna. However, the MM is usually used only for electrically small systems due to the computer resources required to perform the simulation. A test vehicle that has dimensions on the order of several wavelengths poses a considerable computational challenge in terms of both memory and computation time.

Using multiple methods of simulation on one system has brought about "hybrid" simulation techniques. Hybrid techniques, in the general sense, implement a particular method to solve one part of a problem while using another method to solve a different part. The solutions are then brought together to try and accurately represent the actual system. In this way, a technique that is more accurate can be used where accuracy is needed while a technique that is less computationally expensive can be used at different locations that would otherwise require too many resources. There are numerous software packages and computer codes that use a wide variety of methods to simulate an electromagnetic system. A few of these include, NEC [7], ESP [8], WIPL [9], MOM3D [10], JUNCTION [11], FEKO [12], FASANT [13], EMC-2000 [14] and

HEMCUVI [15]. For this study, because of its versatility and availability, FEKO is the software package used.

3.2 The Method of Moments

By the MM technique, an approximation of the current induced over the vehicle is obtained as the numerical solution of an integral equation. This is done in the form of a series of known basis functions [16]. The fundamental idea behind the method will be described to give background for the theory of using hybrid methods.

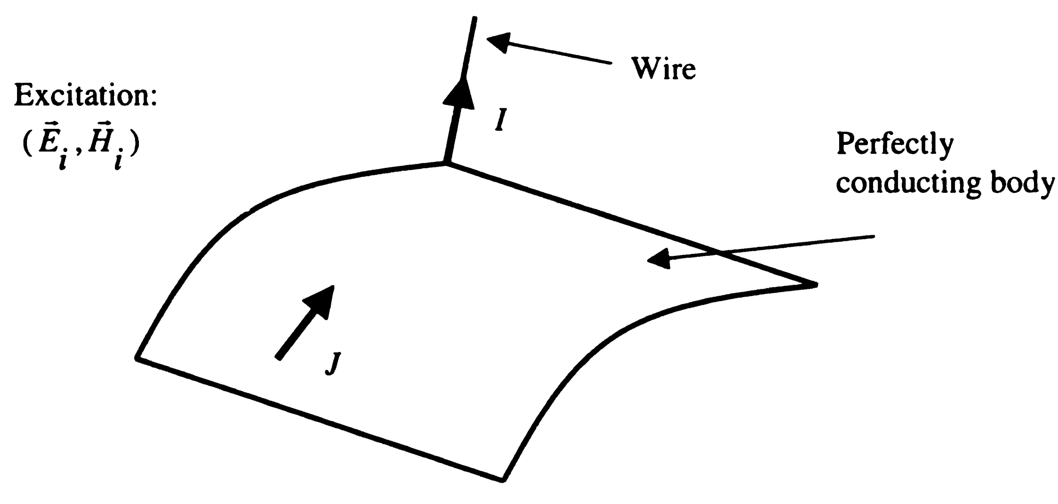

Figure 3.1: Scattering Problem

The theory of MM is widely understood among computational electromagnetics engineers. This particular development and notation is based on [17] since those authors have played some role in the implementation and formulation of the MM in FEKO.

Consider a wire attached to a perfectly conducting surface as shown in Figure 3.1. An incident plane wave is formed by the fields ($\vec{E}_i, \vec{H}_i$) and acts as an excitation to the system. This plane wave induces electric current both on the wire segment (I) and along the perfectly conducting surface in the form of surface currents ($\vec{J}$). These currents are in return responsible for the resulting scattered fields $\vec{E}_S$ and $\vec{H}_S$. Superimposing the incident and resulting scattered fields gives the total fields in the region $\vec{E}_{total}$ and $\vec{H}_{total}$

$$\vec{E}_{total} = \vec{E}_i + \vec{E}_S, \tag{3.1}$$

$$\vec{H}_{total} = \vec{H}_i + \vec{H}_S. \tag{3.2}$$

The scattered fields resulting from the induced current on the wire and surface current on the perfect electrical conducting body (PEC) can be represented by taking the linear integro-differential operator on the surface current $\vec{J}$ and the line current I. This is accomplished by using the operators

$$\vec{L}_J^E\{\vec{J}\} = \frac{-j}{4\pi\varepsilon\omega}\vec{\nabla}\iint_{A'}(\vec{\nabla}'_A \cdot \vec{J}(\vec{r}')) \cdot G(\vec{r},\vec{r}')dA' - j\omega\frac{\mu}{4\pi}\iint_{A'}\vec{J}(\vec{r}') \cdot G(\vec{r},\vec{r}')dA', \tag{3.3}$$

$$\vec{L}_J^H\{\vec{J}\} = \frac{1}{4\pi}\vec{\nabla} \times \iint_{A'}\vec{J}(\vec{r}') \cdot G(\vec{r},\vec{r}')dA', \tag{3.4}$$

$$\vec{L}_I^E\{I\} = \frac{-j}{4\pi\varepsilon\omega}\vec{\nabla}\int_{L'}\frac{\partial I(\vec{r}')}{\partial l'} \cdot G(\vec{r},\vec{r}')dl' - j\omega\frac{\mu}{4\pi}\int_{L'}I(\vec{r}') \cdot \hat{l}' \cdot G(\vec{r},\vec{r}')dl', \tag{3.5}$$

$$\vec{L}_I^H\{I\} = \frac{1}{4\pi}\vec{\nabla}\times\int_{L'} I(\vec{r}')\cdot\hat{l}'\cdot G(\vec{r},\vec{r}')dl'. \tag{3.6}$$

The unit vector $\hat{l}'$ denotes the direction of current flow I along the wire segment. The vector $\vec{r}'$ denotes the location of the observation point. The surface divergence over the primed coordinate system is denoted by $\vec{\nabla}_{A'}$ and $G(\vec{r},\vec{r}')$ is the free space Green's function defined as

$$G(\vec{r},\vec{r}') = \frac{e^{\frac{-j2\pi}{\lambda}\left|\vec{r}-\vec{r}'\right|}}{\left|\vec{r}-\vec{r}'\right|}\ . \tag{3.7}$$

When these operators are applied in the proper form, they yield the scattered fields due to the line and surface currents:

$$\vec{E}_S = \vec{L}_J^E\{\vec{J}\} + \vec{L}_I^E\{I\}\ , \tag{3.8}$$

$$\vec{H}_S = \vec{L}_J^H\{\vec{J}\} + \vec{L}_I^H\{I\}. \tag{3.9}$$

In the moment method, the current $\vec{J}$ is expanded into a series of basis functions $\vec{f}_1, \vec{f}_2, \ldots \vec{f}_{N_J}$ on the perfect conducting surface. The current I is expanded into a series of basis functions $g_1, g_2, \ldots g_{N_I}$ on the wire. When these basis functions are superimposed and weighted by the complex coefficients α_n and β_n they yield an expansion of the currents [18]:

$$I = \sum_{n=1}^{N_I}\beta_n\cdot g_n\ , \tag{3.10}$$

$$\vec{J} = \sum_{n=1}^{N_J} \alpha_n \cdot \vec{f}_n \, . \tag{3.11}$$

In FEKO, the geometry is divided into triangular patches to form a mesh. This allows the choice of the surface current basis functions $\vec{f}_n$ developed by Rao,Wilton and Glisson [19]. A separate basis function is usually chosen for the linear current basis function g_n and is taken here to be a triangular function. FEKO uses special basis functions to transition between the wire segment and the surface. The choice of coefficients α_n, and β_n is determined by considering the boundary conditions to satisfy Maxwell's equations. The vanishing tangential electric field on perfect electrically conducting surfaces is one such condition that can be used [17]:

$$\vec{E}_{\tan} = 0 \tag{3.12}$$

Using this boundary condition, an electric-field integral equation (EFIE) can be derived from

$$\hat{n} \times \vec{E}_{total} = 0 \, . \tag{3.13}$$

Here, $\hat{n}$ is the unit normal vector to the surface in Figure 3.1.Substituting equation (3.1) into (3.8) yields

$$\hat{n} \times \left(\vec{E}_i + L_J^E\{\vec{J}\} + L_I^E\{I\} \right) = 0 \, . \tag{3.14}$$

Inserting equations (3.10) and (3.11) into (3.14) results in

$$\hat{n} \times \left(\sum_{n=1}^{N_I} \beta_n \cdot \left(\vec{L}_I^E\{g_n\} \right) + \sum_{n=1}^{N_J} \alpha_n \cdot \left(\vec{L}_J^E\{\vec{f}_n\} \right) \right) = -\hat{n} \times \vec{E}_i \quad . \tag{3.15}$$

This formulation can be used to solve for the scattered electric field by finding the proper weighting coefficients α_n and β_n. These linear equations have a total number of unknowns $N_{total} = N_I + N_J$.

3.3 Physical Optics

Physical Optics is another commonly employed method for simulation. It is based on the idea that certain areas in a structure are illuminated while others are shadowed. In the illuminated region the PO approximation for currents can be made. In the shadowed regions, only diffraction terms are used. An operator for the PO can be made just as for the MM. Using these approximations allows the basis functions chosen to represent the currents to be greatly simplified and can also reduce the number of unknowns. This reduction, since it is based on an approximation, can affect the accuracy of the calculated fields, so it must be used carefully.

In the illuminated region, the PO approximation can be made for the current density $\vec{J}_{PO}$ flowing on the surface. This approximation is based on the Physical Optics current in the radiation integral [20]

$$\vec{J}_{PO} = 2\hat{n} \times \vec{H}_i. \tag{3.16}$$

Here, $\hat{n}$ is the unit normal vector from the surface and $\vec{H}_i$ is the incident magnetic field. The radiation integral can form an operator just as in the MM case. PO, however, cannot be applied to line currents I as successfully as the MM can. Therefore, a linear integro-differential operator is used only for the surface current

$\vec{J}_{PO}$. This operator is the same as in the MM case (e.g. equation 3.3 and 3.4) but it is used on the currents approximated by (3.16).

3.4 Hybrid Methods

Hybrid methods use one simulation technique at one location while using another technique at a different location. There are several hybrid techniques employed in a variety of software applications [7-15]. The techniques described here are the ones that are most applicable to those used in FEKO. The exact means for implementation of the methods in FEKO are proprietary to the developers so a general description is given.

It is desired, by the use of these techniques, to reduce the total number of unknowns $N_{total} = N_I + N_J$. By making a significant reduction in the number of unknowns, the size of the system of equations can be reduced. Reducing the size of the system of linear equations can greatly reduce the computational cost expended to form a solution. A reduction using PO can only be applied to N_J since the PO approximation cannot be applied to the line currents. Many authors have explored the reduction of computational cost by hybrid methods, including [15].

Using the conventional MM solver, the computational cost in terms of memory requirements is on the order of the total number of unknowns squared, N_{total}^2. The cost in terms of solution time can be as large as on the order of N_{total}^3. If the hybrid method is used then a region is designated as using the MM technique and thus has unknowns N_{MM} and a region is designated as using the PO approximation with unknowns N_{PO}. The number of unknowns, N_{total}, can be expressed as $N_{MM} + N_{PO}$. The PO region is typically much larger than the MM region so $N_{MM} << N_{PO}$. This is because it is recommended that only the regions containing the antenna, near regions, discontinuities and electrically small objects be considered with the MM [15]. The remaining geometry can be considered with PO. The number of PO unknowns can be broken into two separate unknowns N_{PO}^{lit} and N_{PO}^{unlit}

$$N_{PO} = N_{PO}^{lit} + N_{PO}^{unlit} . \tag{3.17}$$

These unknowns are associated with the areas that are illuminated or in a shadow in the PO approximated region. Since $N_{MM} << N_{PO}$, the number of unknowns can be approximated by $N_{total} \approx N_{PO}$. The computational cost associated with the system in terms of storage can be approximated as being on the order of $N_{MM} \cdot N_{PO}^{lit}$ [15]. The relative cost of the MM-PO hybrid compared to a full MM simulation can be represented as the ratio of MM unknowns to the number of PO unknowns:

$$\frac{Cost_{hybrid}}{Cost_{MM}} \propto \frac{N_{MM}}{N_{PO}} \tag{3.18}$$

The hybrid method expresses the PO approximated surface current as a superposition of basis functions $\vec{f}_n$:

$$\vec{J}_{PO} = \sum_{n=N_{MM}+1}^{N_{MM}+N_{PO}} \gamma_n \cdot \vec{f}_n . \tag{3.19}$$

Here, γ_n is the coefficients that are based on the approximation of PO on the surface. Applying the Electric Field Integral Equation as in equation (3.14) but this time including the PO approximated surface current yields equation (3.20).

$$\hat{n}\times\left(L_J^E\{\vec{J}\}+L_I^E\{I\}\right)=-\hat{n}\times\left(\vec{E}_i+L_J^E\{\vec{J}_{PO}\}\right) \tag{3.20}$$

By applying the proper weighting functions, as in the MM, this equation can be converted into a system of equations that can be solved by back-substitution or any other computationally efficient method. This is the fundamental idea for how a PO-MM hybrid method is implemented in FEKO.

3.5 Simulation with FEKO

The program FEKO, which will be discussed in the following sections, is installed on two Hewlett-Packard (HP) J7000 UNIX Workstations. These workstations each have 8 Gb of RAM and four processors that operate at a clock speed of 440 MHz. The FEKO program is a parallel version in that it can coordinate both machines to work together to make computations. This allows a total RAM allocation of 16 GB and a total number of processors in use to be eight. Of course, not all 16 GB of RAM can be allocated in this system since memory is necessary to run the operating system and other incidental applications that may be in use. Realistically, the largest RAM that can be allocated for solving a problem in this system is 13 GB. A larger allocation is possible, but doing so slows the system down so much that the computational cost is too large and a solution cannot be found in a reasonable amount of time. This is believed to be mostly due to the operating system as well as the program itself requiring some additional memory to perform the operations. A problem that requires a very large RAM allocation, that is greater than the available RAM on the computers, can be solved "out of core." An out of core solution writes memory to the hard disk and treats it as virtual memory. Since a hard disk has a very slow read and write ability, it is difficult to find a solution by this method in a reasonable amount of time. An in-core solution is the most practical to solve. This is because an in-core solution only allocates memory to RAM. The RAM has the fastest write and read abilities. Since MM solutions are very memory-intensive, most of the time required for a simulation is due to the movement of memory. For most simulations, if a problem needs to be solved out of core than it is deemed impractical to solve. For all the simulations used in this study, an in-core solution was used.

A small geometry Method of Moments simulation is used to test the parallel processing capabilities of the two HP J7000 computers. The test simulation has 3,100 metallic triangles that form the mesh and 4,506 metallic edges that form these triangles. The total number of basis functions necessary is 4,514 (4,506 edges + 8 wire segments for the monopole). The problem in total requires 350 MB of RAM. The results are shown in the form of the speed-up factor in Figure 3.2. Here $t(n)$ represents the time it takes to complete the same simulation using n processors.

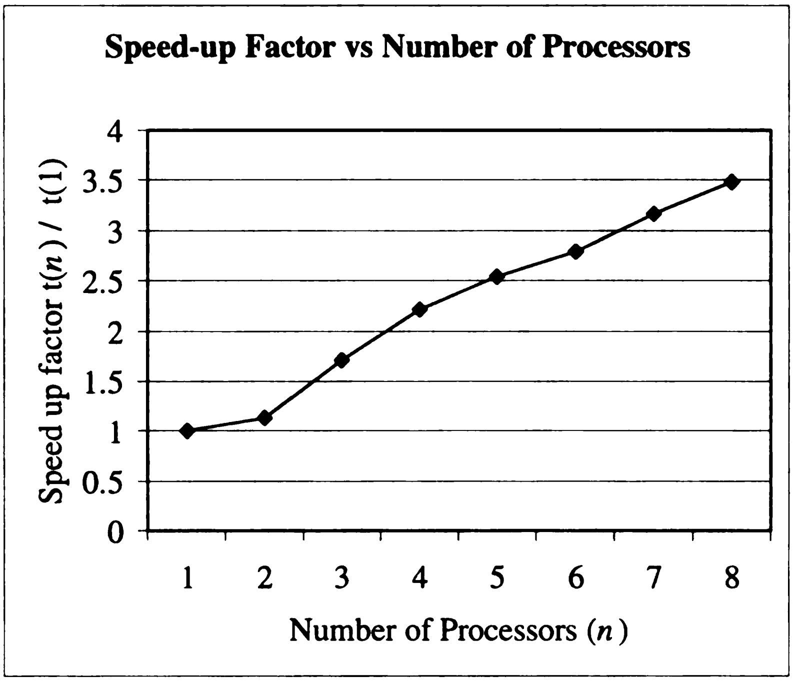

Figure 3.2: The speed-up factor vs. the number of processors

The t(1) term represents using just one processor to complete the job. Using all 8 processors, however, does not allow the problem to be solved 800% faster as might be expected. It is shown that using 8 processors t(8) / t(1) yields a speed up factor of roughly 3.5. This is due to overhead in handling the memory on the 1.3 Gb/s maximum throughput bus and managing the processors to work together.

3.5.1 Introduction to FEKO

FEKO [3] is a software package based on the Method of Moments. The word FEKO is formed from the German acronym for words that translate to "Field Computations Involving Objects of Arbitrary Shape." FEKO is referred to as a software package because it contains multiple programs that are used to take an input from a user, perform a simulation, and view the results. These subprograms are editFEKO, preFEKO, winFEKO, the FEKO solver and graphFEKO. The user steps through the programs to take a problem from the specification to the final results. Taking these multiple steps helps the user realize any errors in the geometry, excitation, or requested fields before an erroneous simulation is committed to run for a long period of time. Since there are 5 programs and about 40 different file types associated with FEKO, only the fundamentals of the programs as well as a few of the important file types will be discussed.

The program editFEKO is used to simplify the creation of an input file. This input file is of the type *.pre and is based on text entries. The *.pre name represents that the "*" could be an arbitrary name. For example the file could be named vehicle.pre. This program has many useful tools to insert commands and organize the text-based input. The program's inputs are all based on "cards." There are only two classifications of cards in editFEKO. These are the geometry cards and the control cards. The geometry cards, as the name implies, are used to specify the geometry of the problem. The control cards are used to specify the excitation, requested fields and other control-type operations. For example, it is also necessary in the program editFEKO to specify the maximum length of a segment in the geometry. This is done through a geometry card since this impacts the geometry of the problem. The maximum length of a segment should be less than $\lambda/10$. According to the FEKO manual, a maximum segment length could be as large as $\lambda/5$ to $\lambda/6$. However, this could lead to severe inaccuracies in the MM solution and should be checked with a smaller segment length anyway. Instead of using many geometry cards to specify a complex geometry such as an automobile, editFEKO can input a variety of geometries from other computer aided design (CAD) programs. Once the problem is completely specified in editFEKO, it is necessary to run preFEKO.

The program preFEKO takes the *.pre file created in editFEKO and prepares it to be viewed as a geometrical problem with an excitation in winFEKO. This is done by the creation of a *.fek file. The software preFEKO also checks the geometry, excitation and requested fields for errors or inconsistencies that would not allow the solver to function properly. The program also summarizes the total number of triangles formed by the segments, the total number of wire segments, and other useful information pertaining to the problem. Once preFEKO is run and the *.fek file is created, the problem is ready to be viewed in winFEKO.

The program winFEKO is a graphical program that allows the problem to be viewed. A verification of the geometry, as well as the proper direction of the normal vectors can be made. It is important for the normal vectors to all face outward on a closed body, for example, since this allows other methods of simulation, such as PO, to be easily applied. The program does not have the ability to change the geometry however since this can only be specified in editFEKO. Once the geometry has been viewed and verified to be correct, the FEKO solver is run which actually performs the simulation. The solver creates the final output in a *.out file. When this is complete the results can be displayed in winFEKO as a three-dimensional radiation pattern. Other outputs of interest, such as current density, can also be displayed in winFEKO. The results can also be interpreted in graphFEKO when it is necessary to compare only certain angles, polarizations, or how well the antenna is matched. In this way, any problem can be specified and the proper steps can be taken to move the problem through the software package to gain a solution. Figure 3.3 illustrates the basic flow of the problem from user input to the program output that is interpreted by the user.

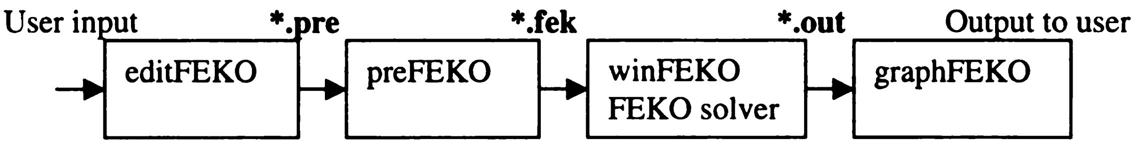

Figure 3.3: The programs and their inputs and outputs

3.5.2 FEKO and the Test Vehicle

The ultimate goal of this study is to compare the measurements that are taken, as described in Chapter 2, to the simulated results. To do this, the diagram in Figure 3.3 needs to be followed when developing an accurate simulation using FEKO. The first step is to specify the problem in editFEKO. This is a very important step and needs to be done with care. Since a vehicle is a large and fairly complex geometry it is difficult to create this in editFEKO through the use of cards. This is true especially since the geometry needs to be broken into triangular patches that need to share edges and vertices in addition to aligning properly to the measured location on the actual test vehicle. Using another program called Concept, this complicated construction of the vehicle is more easily completed. Concept is simply a CAD program that allows the construction of triangles to be easily manipulated. The data is then formatted for editFEKO and imported. The vehicle is thus constructed only with numerous triangles and no other geometrical shapes such as rectangles. These triangles have a very course segmentation length. In fact, the lengths of the edges of the triangles are probably too large. This is because the vehicle was drawn in Concept to be simulated for a variety of frequencies. Additionally, the triangular area formed by the inside of the edges is probably too large for most frequencies. This is because the amount of current on a segment is assumed to be constant in the MM. If this segment is too large then this assumption may be grossly incorrect. It is therefore necessary to further break the course triangles created in Concept into finer triangles that have some frequency dependence so the constant current assumption can be valid. FEKO states, as mentioned before, that the maximum length of a segment can be is $\frac{\lambda}{10}$ where λ is the wavelength in free space. Additionally, FEKO recommends that the area A of a triangle formed by these segments be less than $\frac{\lambda^2}{70}$. The segmentation rules that are recommended by FEKO are adhered to by all of the simulations unless otherwise stated. These rules are summarized in Table 3.1.

FEKO Segmentation Rule	**Warning**	**Error**
Ratio of the segment length l to the wavelength λ	$\frac{l}{\lambda} > 0.3$	$\frac{l}{\lambda} > 0.5$
Ratio of the segment radius ρ to the segment length l	$\frac{\rho}{\lambda} > 0.3$	$\frac{\rho}{\lambda} > 1.0$
Ratio of the area of the triangles A to the wavelength squared λ^2	$\frac{A}{\lambda^2} > \frac{1}{30}$	$\frac{A}{\lambda^2} > \frac{1}{10}$

Table 3.1: The FEKO segmentation rules. From [3]

Many times, a problem is further simplified due to symmetry. FEKO also has the ability to consider magnetic, electric and geometric symmetry to aid in solving a problem faster and more efficiently. A plane of electrical symmetry is a plane that can be replaced by an electrical wall without changing the field distribution. Electrical symmetry can play a very large part in reducing computational cost to a problem. It should be used whenever possible to make a problem easier. A plane of electrical symmetry is illustrated in Figure 3.4.

This plane of electrical symmetry is representative of the influence the perfect electrically conducting ground has on the system. The outer shell of the test vehicle is symmetric. However, a plane of electric symmetry cannot be used since there is only one monopole antenna on the vehicle and symmetry would create two. Instead, geometrical symmetry can be used for the car body without mirroring the monopole antenna. This can be done down the center from the front of the vehicle to the back. Unfortunately, geometric symmetry does not reduce the number of unknowns in the current basis functions as electrical symmetry does. It does, however, lead to a reduction in computation time when the matrix is determined. This symmetry is illustrated in Figure 3.5. The model is created to be of the exact size of the actual test vehicle (1:1 scale). It is a total of 3.6 meters long and 0.44 meters from the perfect electric ground plane that is below the vehicle, but not pictured in Figure 3.5. After symmetry is applied, the total width is 1.6 meters.

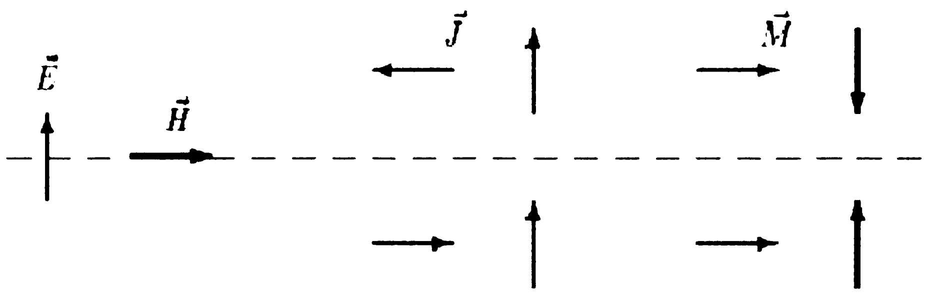

Figure 3.4: The plane of electric symmetry.

The antenna used in the simulation model is a quarter-wavelength monopole with the same length as that of the actual monopole used in measurement. There are five different bands of frequencies for this study. A different quarter-wavelength monopole is used for each frequency band and the lengths are summarized in Table 3.2. Band "Own" has been created specifically for this study.

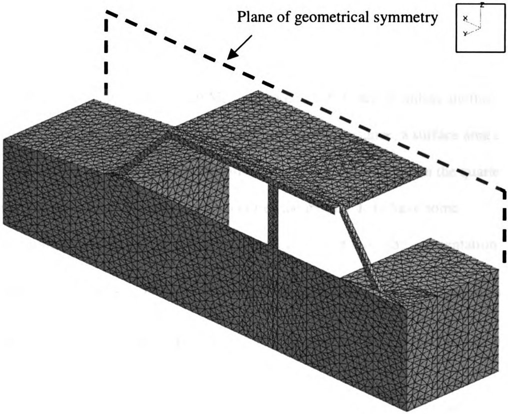

Figure 3.5: One half of the test vehicle. The other half is generated by symmetry.

Band	Start Frequency (MHz)	Center Frequency Used (MHz)	Stop Frequency (MHz)	Monopole Length (cm)
FM	70	90	120	85
3	175	205	235	36
Own	250	350	450	21
4-5	470	670	870	11
GSM	800	900	1000	8.5

Table 3.2: The monopole lengths for simulation

The FEKO solver uses a full MM technique on the vehicle unless another technique is specified by the use of a geometry card. For instance, a surface area could be considered using PO or UTD. Triangular basis functions are used on the quarter-wavelength monopole. The solver thus requires the monopole to have some segmentation that would allow the use of these basis functions. The segmentation for the monopole antennas is the same for the surface mesh and is $\frac{\lambda}{10}$ unless otherwise specified. Once the geometry has been properly represented, the type of excitation needs to be selected.

The program FEKO has 13 different ways of exciting the system. These include excitation by a plane wave, a voltage gap between wire segments, a magnetic current, a voltage along a wire segment and many others. For these simulations, the chosen excitation is by a voltage gap between wire segments. This is most representative of the actual phenomenon that occurs when taking the measurements and is done for all the same frequencies that were measured. Illustrated in Figure 3.6 is a screenshot from winFEKO of the geometry at the feed location. The monopole antenna shown is of length 21 cm and is used for Band Own. Since both the quarter-wavelength monopole and segmentation size both depend on frequency, the monopoles for all five bands each have 8 segments (7 for Band 3). The excitation location is shown as a small hemispherical shell between the antenna and the surface mesh triangles.

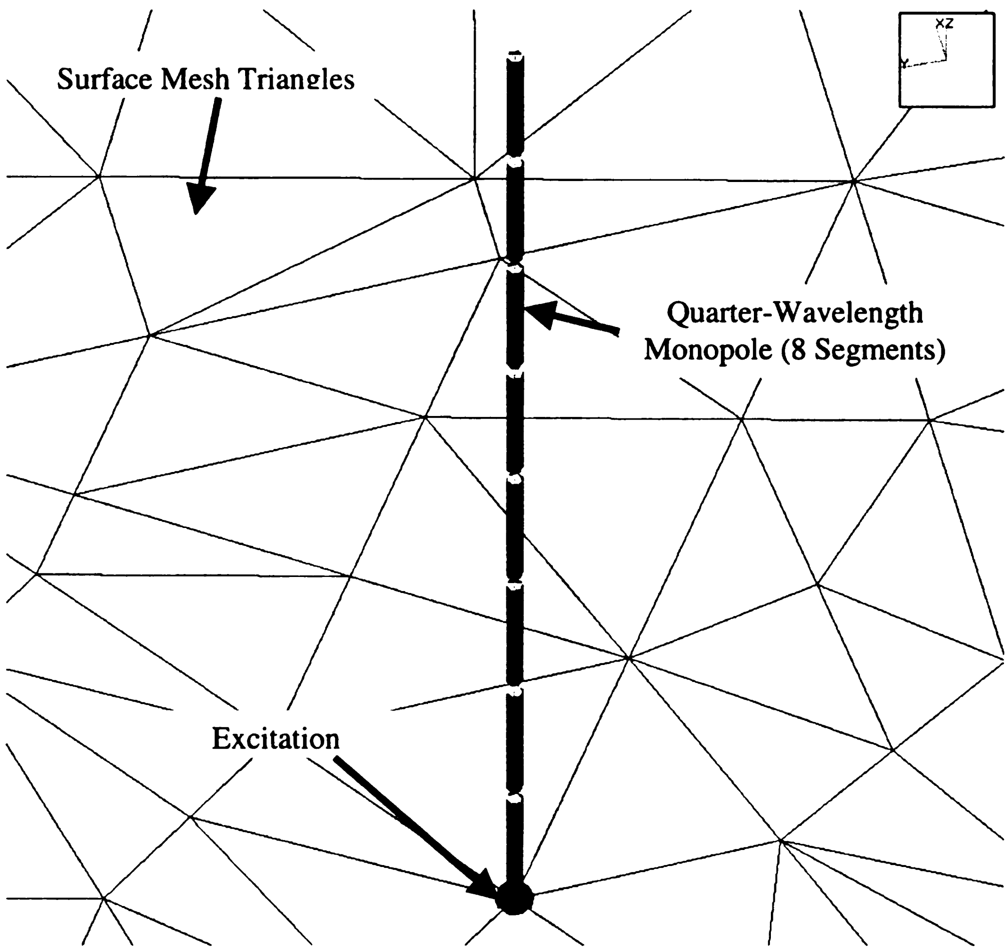

Figure 3.6: The quarter-wavelength monopole, surface mesh triangles and the excitation by a voltage across a gap

The triangular mesh must have a vertex at the point where the monopole is attached as can be seen at the location of the excitation. Once the geometry is correctly verified and the excitation is specified, the final step in setting up the simulation is to identify the "requested fields." This means commanding the software to compute the far field values at all requested locations for all requested frequencies. Again, since the ultimate goal of this study is to compare the measurement to simulation, the requested fields are calculated at the exact locations with the exact frequencies as with the measurements. This is done in spherical coordinates over the entire hemisphere $0° < \phi < 360°$ and $0° < \theta < 90°$. It is not necessary to calculate the field points below the perfectly conducting ground plane since the field values at those locations are zero. The chosen resolution of 2.5° is the same as with the measurements. This means the fields are calculated at 144 points in the ϕ direction and 37 points in the θ direction. This amounts to a total of $144 \cdot (37-1)+1=5185$ locations where the far field values are calculated for both horizontal and vertical polarizations.

Once the geometry is created, the excitation is chosen, and the fields are requested, the simulation is ready for the preFEKO program that creates the *.fek file to be input to the FEKO solver. The preFEKO program also outputs useful information pertaining to the size of the problem. The information for the five bands is summarized in Table 3.3 for a $\frac{\lambda}{10}$ maximum segment length. The $\frac{\lambda}{10}$ segmentation uses the shortest wavelength (highest frequency "f_{upper}") within the band.

Band $(f_{lower} - f_{upper})$	**Number of Metallic Triangles in Free Space**	**Number of Wire Segments in Free Space (from the Monopole)**
FM (70 – 120 MHz)	2,744	8
3 (175 – 235 MHz)	7,600	7
Own (250 – 450 MHz)	17,366	8
4-5 (470 – 870 MHz)	56,054	8
GSM (900 – 1000 MHz)	70,698	8

Table 3.3: The number of metallic triangles and wire segments in free space as output by preFEKO

Once the *.fek file is created, it is important to visually inspect the geometry in winFEKO to ensure that it is correct and the normal vectors are facing in the correct direction. After the visual check in winFEKO, the *.fek file is ready to be processed by the FEKO solver. The FEKO solver uses the MM to compute the surface currents and then uses the integro-differential operators to find the field values at the requested field locations and produces the *.out file. The MM technique has a large RAM consumption and requires significant processor time. The full MM simulation is run for all bands of frequencies with a 2.5° resolution for 51 frequencies. This will allow an exact comparison to measurement. Table 3.4 shows the number of unknowns and the average time per frequency point to run the simulations using all 8 processors.

Band	Number of Metallic Edges (MM)	Number of Basis Functions	RAM Required (MB)	Average Simulation Time per Frequency (hours)
FM	3,972	3,980	258.150	0.032
3	11,256	11,263	1,961.420	0.336
Own	25,882	25,890	10,373.720	3.07
4-5	83,786	83,794	112,042	~30
GSM	105,706	105,713	178,818	~90

Table 3.4: The total memory required and time for simulation

Table 3.4 includes the RAM required for these simulations. In the case of Band 4-5, the RAM is larger than the two HP computers can realistically handle. This simulation takes an unreasonable amount of time to run at the $\frac{\lambda}{10}$ segmentation and therefore is not permitted to finish. For this reason, it is decided to use a $\frac{\lambda}{5}$ maximum segmentation length to lower the computation cost. This is at the largest boundary for acceptable segment lengths according to FEKO and probably does not yield very accurate results. This very course segmentation still has 24940 metallic edges and 24948 basis functions. This requires almost 10 GB of memory and nearly the same amount of time as the Band Own simulation. For Band GSM, there is no way to use even the greatest allowed segmentation of $\frac{\lambda}{5}$ since the required RAM is still too large. So, a maximum allowed length of $\frac{\lambda}{4.525}$ is used. This requires 26422 metallic edges and 26429 basis functions. To accomplish this, roughly 10 GB of memory is required and a simulation time of nearly the same as Band Own. Since this simulation exceeds even the coarsest allowed segmentation rules it is expected that these results will be less accurate than a properly sampled simulation.

3.5.3 Hybrid Methods and the Test Vehicle

The results shown in table 3.4 illustrate the problems associated with simulations that are electrically large using MM. For the given computational abilities, a simulation of the test vehicle for Band FM and Band 3 are indeed quite practical. They require a reasonable amount of RAM (less than 2 GB) and can be completed in about one hour (maximum) for 51 frequency points while maintaining the recommended segmentation lengths. Band Own, however, is nearing the peak of the computing abilities for the HP machines. It requires 10 GB and a full 3 hours to simulate a frequency point. Additionally, Band 4-5 and Band GSM cannot be simulated using the MM in FEKO with the proper segmentation lengths. They are simply too large and require extreme amounts of RAM and computation time. This has brought about the need for a hybrid method of simulation. A hybrid method could incorporate the PO with the MM to reduce the RAM required and hopefully speed up the calculations while maintaining relatively good accuracy. This could ideally allow the Band GSM and Band 4-5 simulation to be possible in addition to making the Band Own simulation less computationally expensive.

A hybrid approach is accomplished in the geometry specification of the simulation process in editFEKO. FEKO has the ability to selectively solve some areas of the geometry with the accurate but computationally expensive MM while using the PO approximation on other areas. As stated in the theory section for PO, the Physical Optics approximation for currents on the body of the vehicle should only be applied to certain areas. First of all, the wire quarter-wavelength monopole antenna must be considered with the Method of Moments since the PO approximation is best applied to surfaces. Additionally, a small plate below the wire antenna should use the MM so the accuracy of the input impedance can be maintained. Often, antenna engineers recommend that the size of the MM region be 2λ or larger to allow a sufficient area for the surface wave on the vehicle to maintain accuracy. However, in the case of the largest frequency of Band Own, the feed plate would need to be $2\lambda = 1.4$ meters. This is nearly as large as the entire rear trunk (1.8 meters). There are also many parts of the vehicle within a distance of 2λ from the antenna such as the pillar and roof. Considering all of these, or even just the entire trunk, with the MM would not allow a sufficient reduction in RAM requirements. Thus, the feed plate is chosen to be much smaller than 2λ with the anticipation that there will still be relatively good accuracy. The feed plate is roughly 20 cm by 13 cm.

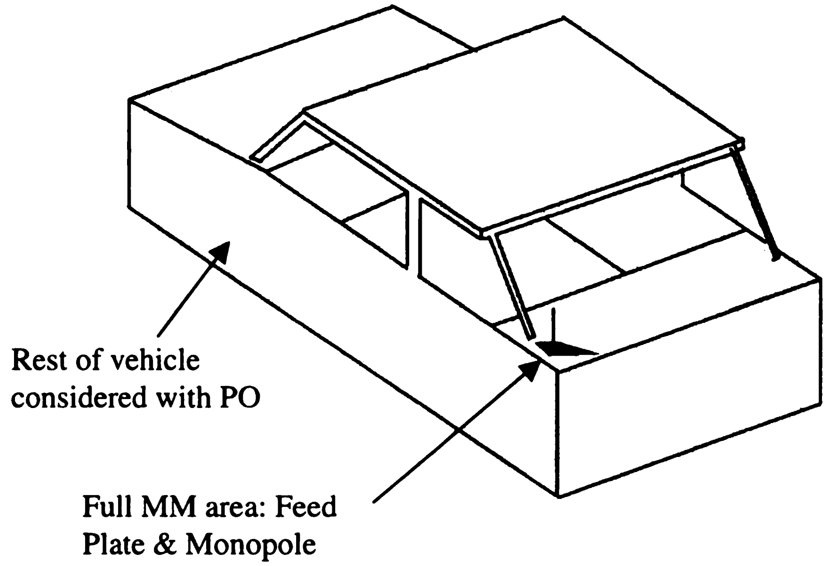

Figure 3.7: The test vehicle with MM feed plate and monopole and the rest of the vehicle considered with PO approximation

Since Band Own is the highest frequency band that can be simulated with a full MM approach on the available computers, it is used most extensively in the approach for hybrid methods. Additionally, due to the very large computation times, simulations here are often done only at a single frequency as opposed to all 51 frequencies. This allows a quick inspection to see if the results appear reasonable, and if so, a more thorough simulation can then be examined. The results are discussed in detail in Chapter 4. The first step in exploring the feasibility of hybrid methods is to consider the entire test vehicle with PO while using the MM on just the wire quarter-wavelength monopole antenna and a small feed plate below the antenna. The area surrounding the MM feed plate and antenna on the driver's side rear trunk and the rest of the vehicle is considered with PO. This is shown in Figure 3.7.

The PO card in FEKO has several options that must be considered. For the first trial, the entire vehicle with PO is used with only the most basic options selected. This is done with "full ray tracing" and "decoupling with moment method." The full ray tracing option traces out the path of a ray from its origin, through any reflections that may occur, and out to the far field. The reflections occur by encountering electrical conducting bodies such as the side, any of the six pillars, or roof of the vehicle [21]. Additionally, as in the full MM simulation, there is an infinite PEC ground below the vehicle. This simulation is denoted here as "Hybrid I" since later it will be easier to reference the simulation results. This is done for the center frequency of Band Own at 350 MHz and is simulated with full ray tracing and decoupling with moment method. Additionally, it is decided that since the computational cost is so low with this PO approximation, that the segmentation length can be further reduced at very little expense. For this reason, a maximum segmentation length of only $\frac{\lambda}{15}$ is used in an attempt to maintain accuracy. For this simulation, 86 metallic edges are considered with the MM while 53,362 metallic edges use the PO approximation. Therefore, 94 MM basis functions and 53,362 PO basis functions are used. This corresponds to a total of 101.236 MB. This is two orders of magnitude smaller than a full MM simulation requirement of 10 GB and represents a remarkable savings. The simulation requires 0.208 hours to complete one frequency point.

The goal of this exploration is to find a reasonable balance between simulation time, accuracy, RAM consumption and practicality. The simulation, taking 0.208

hours per frequency point, when approximated for a full 51 points takes roughly 10 hours. The actual results of the radiation pattern and input impedance of this simulation will be discussed in detail in Chapter 4.

The next step is to consider again the whole vehicle with PO, but this time including coupling the MM region with the PO region. This may be a better assumption since currents in the feed plate certainly affect surface current on the rest of the vehicle. Again, the maximum segmentation length is decreased to $\frac{\lambda}{15}$ to maintain some accuracy. This simulation is denoted as Hybrid II and is run for 350 MHz just as Hybrid I. The simulation requires the same edges and basis functions as Hybrid I. However, there is a much larger memory requirement to handle the coupling of the PO to MM regions. This simulation requires a total of 798 MB. This simulation takes 0.241 hours for the one point. Multiplying this time by 51 gives an approximate total simulation time of about 12 hours.

So far, all the simulations are run with a perfectly electrical conducting ground that is infinite. The Radome, as discussed in Chapter 2, has a conducting ground that is only 24 meters in diameter. Outside the Radome, there is earth ground that is mostly non-conducting. Therefore it is attempted in Hybrid III to model the conducting ground of the vehicle with PO, the entire vehicle with PO and the feed plate and monopole antenna with the MM. The coupling with the MM and PO regions is considered and full ray tracing is used. A large circular conducting disc is used to model the Radome ground. This disc has an extremely large area however, and reducing the radius from 12 meters to 10.2 meters reduces the number of triangles from 288,296 to 222,400. This is a very large number of triangles but a radius of 10.2

meters is used to save on memory. Also, the PO ground uses a maximum segmentation length of $\frac{\lambda}{5}$. This simulation is mainly run for experimentation to see if there is an impact on the input impedance due to the PEC. The number of basis functions for the PO region is 332,811 and the number of MM basis functions is 64. This simulation takes a total of 3592 MB of RAM and 0.780 hours to perform for 350 MHz. The far field radiation pattern is not calculated since this experiment is for input impedance and the far-field radiation pattern would take an extremely long time to compute.

After examining the current density on the vehicle for a full MM simulation, the hybrid currents are compared in Chapter 4. This comparison is valid since the MM simulation is often considered as a benchmark for other simulations. This will also be validated in Chapter 4 also. As for now, the current density acquired by Hybrid I, II, and III is insufficient to yield the proper radiation pattern or the proper input impedance. These are the two most important aspects of this study. Therefore a more advanced hybrid method is employed that is intended to compensate for this inaccuracy. The areas on the vehicle where there are sharp discontinuities yield a lot of current activity as will be seen in the upcoming MM current density results. The density is rapidly changing on the roof edges and at and around the pillars. This rapidly spatially changing current density is not well simulated by the PO approximation. Therefore, it is decided to expand the MM region to include the roof edges and the pillars. Note that part of the roof is also considered with the MM region. This is an attempt to use the more accurate MM approach where there are lots of changes in current density and use the PO approximation where current is less volatile.

This is shown in Figure 3.8 and is represented by Hybrid IV. Hybrid IV uses the $\frac{\lambda}{10}$ segmentation since the number of MM basis functions is increased. The number of triangles is 17,378 and 1,946 metallic edges are considered with MM. There are 23,954 edges that use PO. This requires 6576 MB to complete this simulation. This simulation does consider the far field calculation for five frequency points and takes a total time of 51.830 hours. That makes roughly 10 hours per point and represents a significant increase in computation time.

FEKO has some geometry correction cards that can be used to compensate for inaccuracies with certain canonical geometries for the PO approximations. These cards can, for example, compensate for surface current on two sides of a wedge. Or, the current on the sharp edge of a plate can be better approximated. Since the test vehicle is composed of sharp PEC plates that are interconnected these correction cards can be placed at a variety of locations. For instance, there is a wedge formed by the front bumper of the vehicle and the side panel. This is an example of one of about twenty corrective wedges that are implemented in the vehicle to try and further improve the simulation of the current density and ultimately the far field pattern and input impedance. The other correction card implemented is the current on the edge of a plate. The roof edge and pillars are all simulated using the full MM. This leaves only a few edges that need to be considered with this correction card.

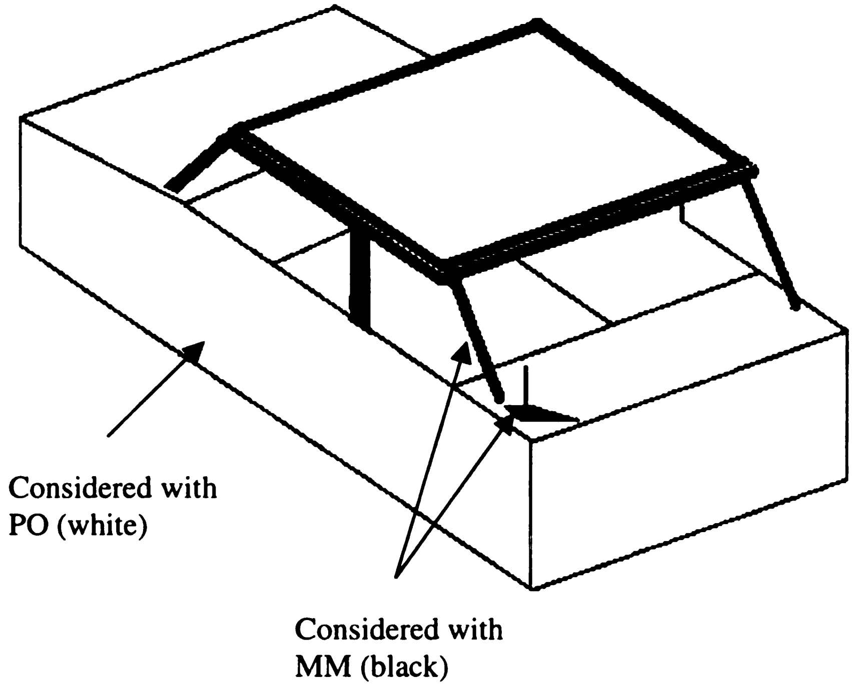

Figure 3.8: The vehicle as considered with Hybrid IV. The roof edges and the pillars are considered with MM (shown in black) and the rest of the vehicle with PO (White)

The driver side door is one example of a location of this corrective edge. There are a total of five corrective edges implemented on the test vehicle simulation model. This simulation uses the $\frac{\lambda}{10}$ segmentation as in Hybrid IV since the same areas are considered with MM. The only difference is the corrective cards. This simulation has similar memory requirements as Hybrid IV since the same areas are considered with PO and MM. The simulation time, however, is different. The total computation time to compute the far-field data at three frequency points is 39 hours. This means a simulation time of roughly 13 hours per point. This represents a 30% increase in time from the simulation Hybrid IV.

The comparison of these simulation results will be explored in detail in Chapter 4. There are many decisions to be made regarding which region to choose as MM and which to use the PO approximation. Additionally, the use of corrective cards to compensate for edge effects has a distinct impact on the overall solution. A few different simulation approaches were discussed here to gain an understanding of how using a hybrid method through the implementation of a surface current approximation can impact the simulation time, RAM requirements, and overall accuracy.

CHAPTER 4

COMPARISON OF RESULTS

4.1 Introduction

Now that the measurements have been described in Chapter 2 and the simulations in Chapter 3, the goal of comparing the separate results can be met. From this comparison some conclusions will be drawn here, and others will be discussed later in Chapter 5. The first comparisons are between the full Method of Moments simulations and measurements. This is because the MM is typically the most accurate means of simulation and is most likely to best match the measurement. Once the MM simulations are compared, the hybrid results will be explored. Since there are three different types of measurements, each will be looked at independently. First, the input impedance will be compared. Next, the far field radiation patterns will be examined and, finally, the transformed far field data will be explored.

4.2 Comparison of Method of Moments and Measurement

The MM simulations, as discussed in Chapter 3, are compared to measurement for all bands including FM, Band 3, Band Own, Band 4-5 and Band GSM. Once a correlation between the MM and measurement has been established, the results of the hybrid methods will be explored. They will be compared with the MM and with actual measurement.

4.2.1 Comparison of Input Impedance Measurement with MM

The input impedance is compared first since it is the most simple, has the least amount of data, and is the most simple to compare. Recall that the impedance is both measured and simulated for the appropriate monopole antenna attached to the top of the left rear trunk of the vehicle. The details concerning the measurement is included in Chapter 2 and the simulation is discussed in Chapter 3. The input impedance is shown on a standard smith chart for all bands. Figure 4.1 includes a comparison of measured impedance for Band FM with MM simulated. The frequency range for this band has been truncated here to 76-108 MHz. This is because this smaller range is used in simulation even though 70-120 MHz is used for measurement. There are still data points at the same frequencies within the 70-120 MHz set and a reasonable comparison can be made. Figure 4.2 shows a comparison for Band 3 between MM and measurement for 175-235 MHz. Figure 4.3 shows the input impedance for Band Own 250-450 MHz. Figure 4.4 shows the input impedance for Band 4-5 from 470-870 MHz. Figure 4.5 illustrates the impedance for Band GSM spanning 800 -1000 MHz.

A very good correlation between the measured and simulated impedance on the test vehicle can be seen for Band FM in Figure 4.1. The simulation impedance curve follows the measurement data with the exception of a very slight shift. A small clockwise rotation in the simulation would allow a better accordance with measurement. However, the curve includes the same general features in simulation and measurement. Additionally, many points are nearly perfectly aligned for frequencies between 95-108 MHz.

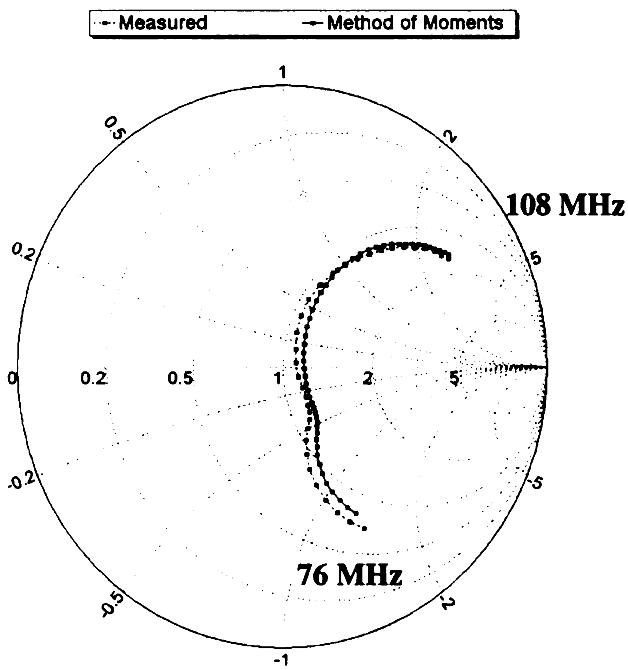

Figure 4.1: Input Impedance for Band FM 76-108 MHz with MM and Measurement

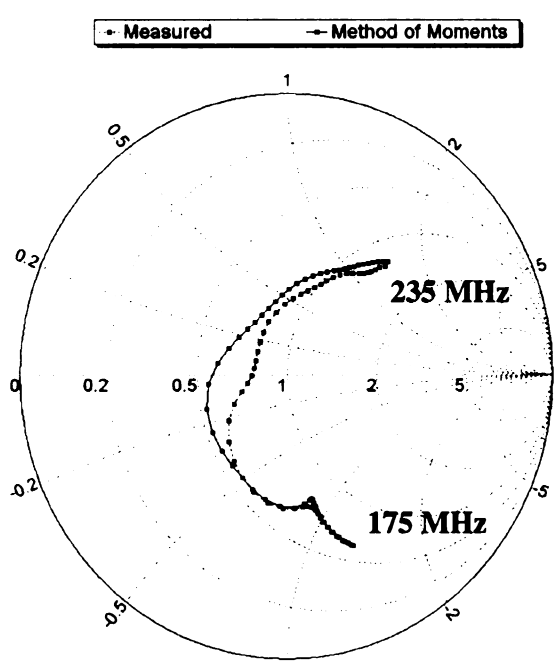

Figure 4.2: Input Impedance for Band 3 175-235 MHz with MM and Measurement

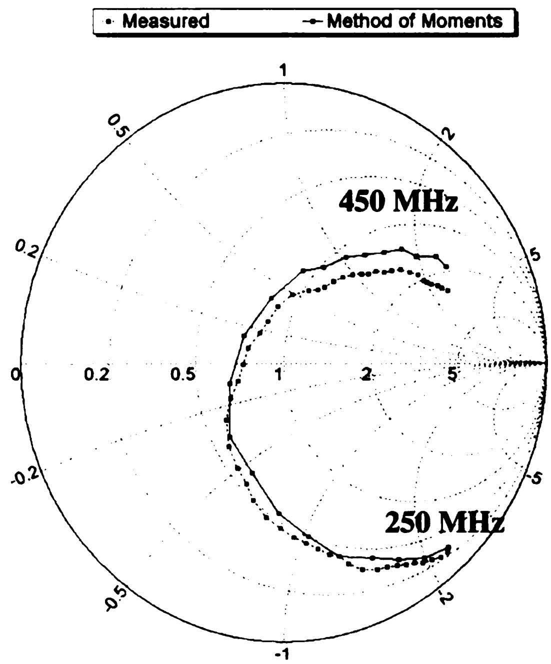

Figure 4.3: Input Impedance for Band Own 250-450 MHz MM and Measurement

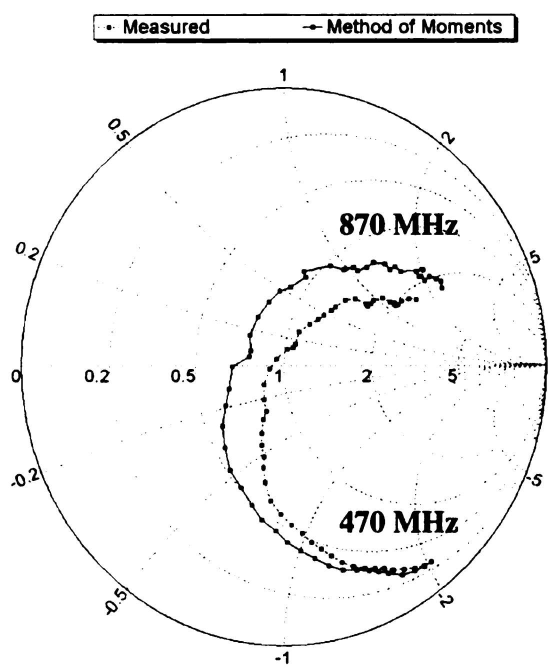

Figure 4.4: Input Impedance for Band 4-5 470-870 MHz MM and Measurement

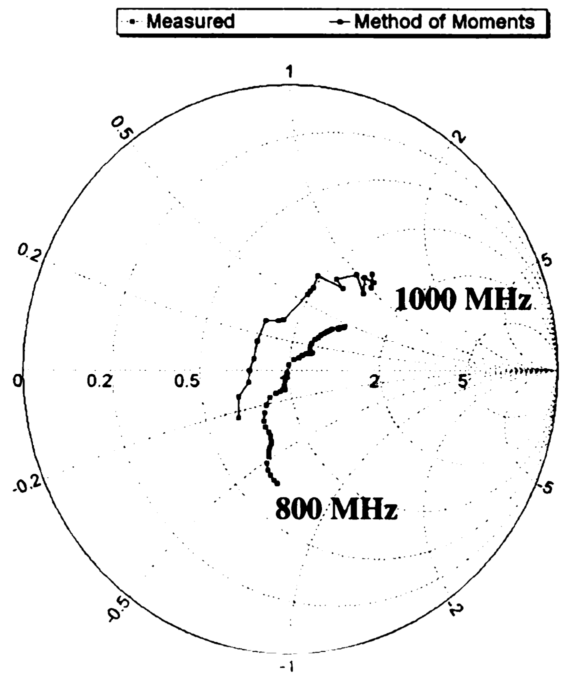

Figure 4.5: Input Impedance for Band GSM 800-1000 MHz MM and Measurement

Figure 4.2 illustrates that there is a fairly good correlation between measurement and MM simulation for Band 3. The points near the upper and lower boundaries of the frequency band (175 MHz and 235 MHz) are close in value. The center frequencies, around 205 MHz, are not as well correlated. There is also a higher concentration of measured data points near the center frequency than in the MM simulation. The simulation has the impedance data points closer together near the outer boundaries of the frequency band. This means that the MM simulates a greater change in impedance with respect to frequency near the center frequency than is shown by measurement. Additionally, the simulated curve is slightly shifted upward from the measured curve for the higher frequencies within Band 3. Thus, the curves share the same basic features and shape, but the actual measurement and simulation points have some small discrepancy.

Figure 4.3 shows a good general comparison of the input impedance between the MM and measurement for Band Own. This comparison is especially important because many of the hybrid methods are also developed in this band of frequencies. Because of the extreme computational requirements to simulate Band Own, only 21 data points are used from 250-450 MHz instead of the measured 51 data points. This is decided since there is not a lot of detail in the measurement curve (no resonance is apparent) and less data points can be used to adequately describe it. As in Band 3, a slight clockwise rotation in the simulated data would allow a very good correlation to the measured data.

Figure 4.4 depicts the impedance curves for Band 4-5. As stated in Chapter 3, the simulation for this band could not be run with the proper segmentation length of $\frac{\lambda}{10}$. This simulation is run with a maximum segmentation length of only $\frac{\lambda}{5}$ and thus the impedance results are not considered to be accurate. Despite this large segmentation, there is still a fairly good accordance with measurement. The lower frequencies, near 470 MHz, appear to have an especially good correlation to measurement. This is probably because the segmentation is chosen for the maximum frequency of 870 MHz. Using a $\frac{\lambda}{5}$ segmentation length with λ solved from the upper bound (870 MHz) yields a maximum length of 0.0689 meters. This length is nearly the same as $\frac{\lambda}{10}$ for the lower bound (470 MHz), which yields 0.0638 meters. Therefore, the proper segmentation length is nearly satisfied for 470 MHz but is not for 870 MHz.

Figure 4.5 illustrates the Band GSM impedance curves for measurement and simulation. The measured results are interesting because of the resonance in the curve. This is usually difficult to accurately simulate. Again, however, the MM segmentation rules cannot be satisfied. The memory required for this simulation is simply too great and a segmentation length of even greater than $\frac{\lambda}{5}$ is used, as described in Chapter 3. Therefore it is determined that the simulation results are mostly meaningless for Band GSM. This again points to the need for hybrid methods to allow higher frequency simulations to be run.

Overall, the impedance results between the MM and measurement are very good. This is especially true when the segmentation rules can be properly satisfied. There is a trend of a slight rotation and shift between the measured and simulated curves. Though it may be difficult to determine the exact cause of this shift, one possibility could be some small electrical delay that is not accounted for in measurement. This could have allowed a phase error. The network analyzer is calibrated before any measurements are taken but the use of a small adapter that could not be accounted for may be a reason for this shift. This would assume that the MM simulation is indeed more accurate than the measurement itself. The possibility that the maximum segmentation length $\frac{\lambda}{10}$ is not small enough is not very likely to be a cause for this error. This is indicated because the same simulation for Band FM and Band 3 with a $\frac{\lambda}{20}$ maximum segmentation length is run and the results yield nearly the exact same impedance curve. So, since the presumably more accurate $\frac{\lambda}{20}$ segmentation length simulation yields the same results as the $\frac{\lambda}{10}$ segmentation length simulation, it can be assumed that the $\frac{\lambda}{10}$ simulation is accurate. Another possibility is that FEKO needs a different choice of basis functions for transitioning between the wire segments and the surface. This is the area with the most current activity and where the impedance is actually determined. This would assume that the measurement is more accurate than the simulation. The impedance results in general are very good. When the segmentation rules are properly satisfied, it would be relatively safe for an automotive engineer to assume that the MM simulated impedance is very close to measurement.

4.2.2 Comparison of Far Field Measurement with MM

The far field radiation measurements and simulations are very important for this study. Recall from Chapter 2 that the far field measurements are taken by rotating the vehicle 360° while a signal is broadcasted from an antenna 100 meters outside the radome. This is done for only one elevation angle but for both horizontal and vertical polarization (FFH and FFV). The elevation angle is estimated to be about 85°. This is decided because the 85° cuts of both the horizontal and vertical polarization radiation patterns from simulation best match the measurement patterns. The scale for the figures shown for these plots is a normalized amplitude scale from 0 to –40 dB. This is because the received voltage in measurement may not be in the same range as what is simulated. However, the relative received signal strength may be proportionally equivalent to simulation if the results are normalized so that the peak measured signal strength is set to 0 dB for both measurement and simulation. The horizontal polarization plots usually have more detail (numerous nulls) than the vertical polarization plots. This is especially true for the lower frequencies. This is because the antenna on the vehicle is vertically aligned and receives horizontally polarized components through coupling with the vehicle.

Shown in Figure 4.6 are the full MM simulation results for the FM band center frequency of 92 MHz with the far field measured results for both vertical and horizontal polarizations. Only the center frequency is shown to save space but this measurement and simulation are performed for many other frequencies in the band as previously described. Note that the front of the vehicle is facing 0° and is depicted in gray in the plots. There is an excellent accordance between measurement and simulation for this frequency for both polarizations. The general shape of the FFV plot is followed but this has very little detail for 92 MHz. The FFH plot shown in the bottom of Figure 4.6 is more interesting since it has a few nulls at 30°, 85°, 150°, 325° and some detail near 255°. Not only does the simulation accurately capture the measured locations of these nulls, but also properly represents the depths. The other frequencies in this band show similar results. This figure is a good representation of the entire frequency band so only 92 MHz is shown.

Shown in Figure 4.7 are the full MM simulation results for the center frequency of band 3 (205 MHz). This figure also includes the far field measured results for both vertical and horizontal polarizations. As in the FM band, there is a very good correlation between the measured and simulated results. The general shape of the vertical polarization curve is the same in both measurement and simulation. The horizontal plot contains a lot more detail. There are several nulls in the simulation that are similar to the measured results. The depths of the nulls are slightly deeper in simulation than in measurement however. For instance at about 330° there is a null in simulation that has a normalized magnitude of –20 dB and the measured value is –10 dB. The location of the null itself is consistent however. Both the horizontal and vertical polarization plots show a good match between measurement and simulation.

Figure 4.8 illustrates the FFV and FFH plots for the center frequency of band Own at 350 MHz. Again, the results are fairly good between measurement and simulation. It can be seen that the number of nulls is starting to increase as higher frequencies are investigated. The FFV plot includes some nulls in the first quadrant $0° < \phi < 90°$. These nulls are captured in measurement and simulation. The angles between $300° < \phi < 345°$ seem to have some slight discrepancy in amplitude but the general features are similar. This may be a difficult region to make the results match since the antenna is mounted on the rear left trunk top and these angles are the front right side of the vehicle. Thus, the vehicle itself is partly shadowing the antenna. Overall, however, there is a good enough correlation for an engineer to rely on the MM simulation. The results for other frequencies in this band are similar.

Figure 4.9 contains the FFV and FFH for band 4-5. This includes simulation and measurement. At 670 MHz, there are quite a few nulls in the radiation patterns for both vertical and horizontal polarizations. The simulation for this band however uses the lower bound for the acceptable maximum segmentation length. Therefore, it is assumed that the many discrepancies between measurement and simulation are largely due to the lengths of the triangle edges being too large. Using some imagination, if the nulls in simulation were less deep, then the measured results would start to look similar for the FFV plot. The simulation nulls are slightly too deep for the FFH scenario but there is a much smaller error between measurement.

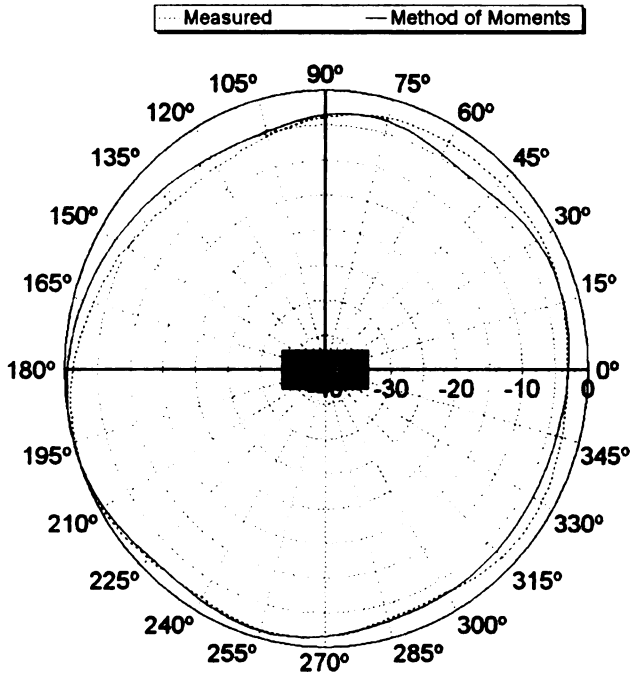

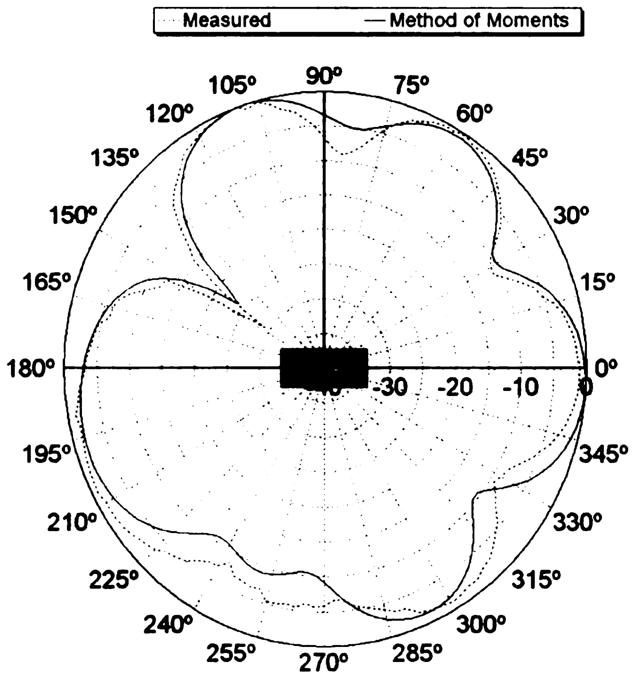

Figure 4.6: Band FM Far Field Measured for Vertical (Top) and Horizontal (Bottom) Polarization Shown with MM Simulation for 92 MHz and Vehicle Facing 0° (Shown with Normalized Amplitude dB)

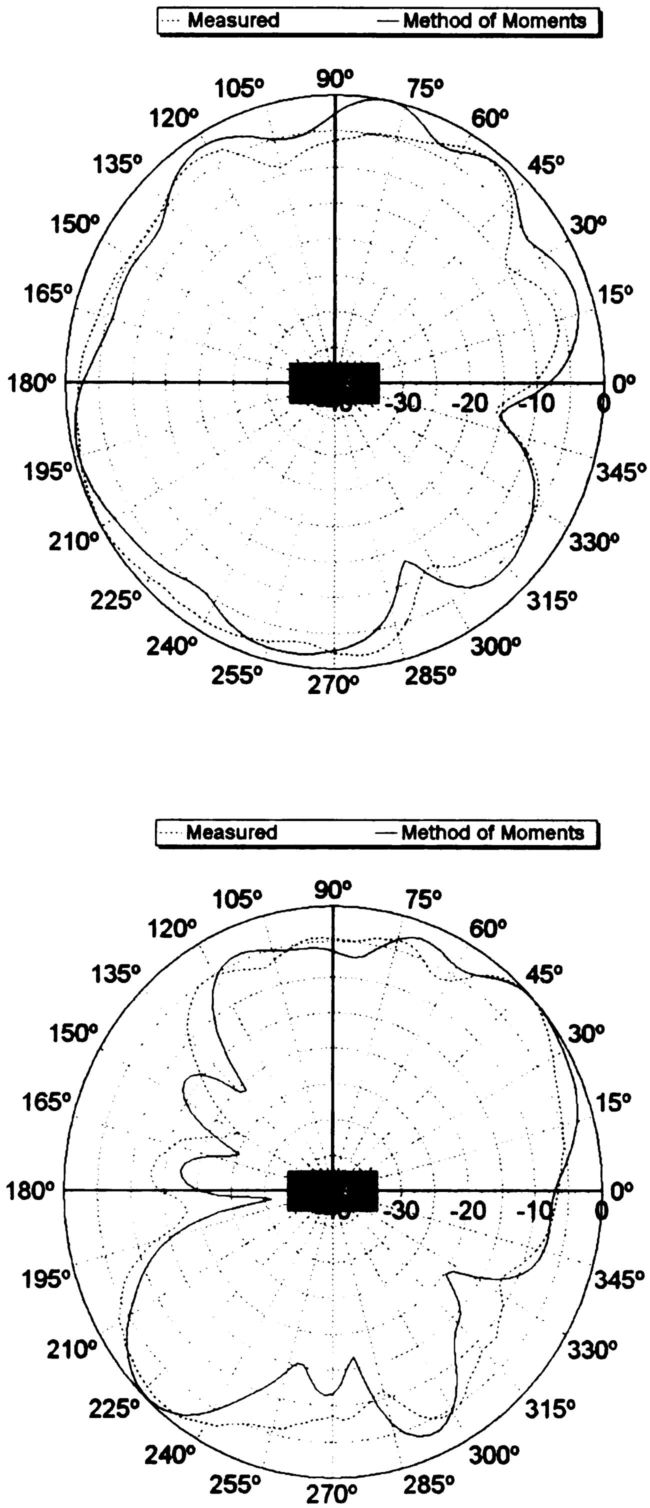

Figure 4.7: Band 3 Far Field Measured for Vertical (Top) and Horizontal (Bottom) Polarization Shown with MM Simulation for 205 MHz and Vehicle Facing 0° (Shown with Normalized Amplitude dB)

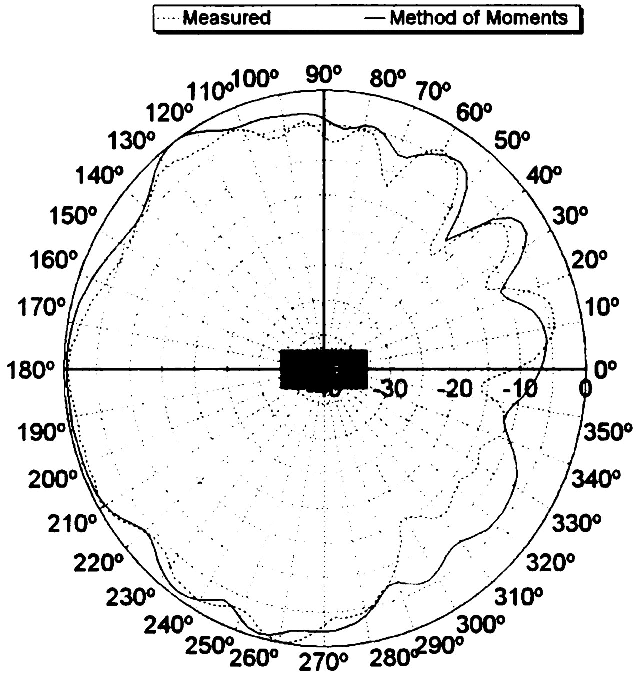

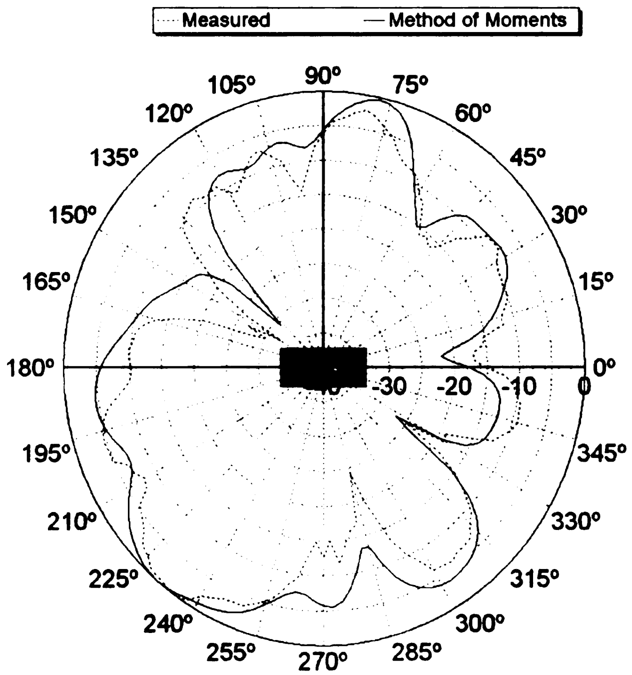

Figure 4.8: Band Own Far Field Measured for Vertical (Top) and Horizontal (Bottom) Polarization Shown with MM Simulation for 250 MHz and Vehicle Facing 0° (Shown with Normalized Amplitude dB)

Using some imagination, if the nulls in simulation were less deep, then the measured results would start to look similar for the FFV plot. The simulation nulls are slightly too deep for the FFH scenario but there is a much smaller error between measurement. The overall features of the FFH plots are similar for most frequencies within this band. At the higher frequency range of 870 MHz, there is not a very good correlation between measurement and simulation because the triangle segment lengths are getting larger with respect to the frequency at that point and a good representation of the surface current is not made.

The band GSM plots for FFV and FFH are not shown here since the segmentation rules are violated in the MM simulation. This yields a radiation pattern that is mostly meaningless. A comparison cannot be accurately made and no conclusions can be drawn from this plot so it is not included.

The comparison of FFV and FFH measurements to the method of moments simulation results shows that the MM is a very good means to estimate the performance of an antenna. This has only been shown here for the elevation angle of 85° but demonstrates that the measured far field radiation pattern is consistent with simulation and can be used later to compare with the transformed near field to far field data.

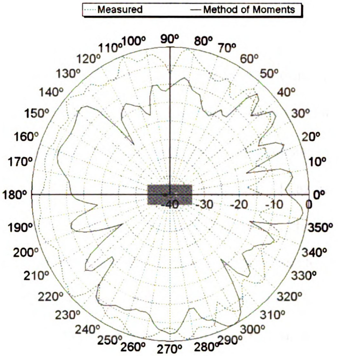

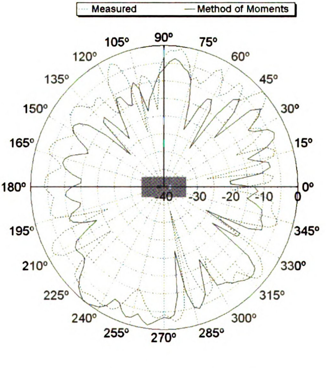

Figure 4.9: Band 4-5 Far Field Measured for Vertical (Top) and Horizontal (Bottom) Polarization with MM Simulation for 670 MHz and Vehicle Facing 0° (Shown with Normalized Amplitude dB)

4.2.3 Transformed NF-FF Measurement with MM Simulation

The comparison of the MM simulation is now done with the far field results that are transformed from near field data. This near field measurement and transformation is described in Chapter 2. This comparison is very extensive since it involves more than just one 360° rotation at a single elevation angle. The NF-FF transformed data contain 74 different elevation angles and 144 azimuth angles. There are clearly too many plots to include here. Therefore, cuts are chosen that are representative of the performance of the simulation with respect to the measurement. This comparison will focus on the results for band Own. This is because band Own is the highest frequency range that can be simulated with the proper segmentation of the vehicle and antenna with the given computational resources. This will also allow the study of the hybrid methods results to be an easy extension of this comparison.

Shown in Figure 4.10 is the vertical and horizontal polarization plots of the radiation pattern for $\phi = 0°$ for the center frequency of band Own (350 MHz). It can be seen that for this angle the MM simulation does fairly well at representing measurement. The most noteworthy discrepancy is at the angle $\theta = 65°$ for the horizontal polarization. There, a deep null in simulation and only a slight null in measurement can be seen. A null is also evident at $\theta = 40°$ in the vertical polarization. It is common that the measurement null depth is not as sharp as the simulation depth. This could be due to reflections and noise in the radome. This would allow some signal strength to be measured when it is not from the actual test antenna. Of course, this would not be simulated, allowing the simulated null depth to be much more profound. The transformation from near field data to far field data uses the values last measured to approximate the immeasurable points down near $\theta = 85°$. The choice to use the last values measured as opposed to just filling these measurements with zeros is governed by observing that the simulated results show a peak at the vertical polarization plot of about –1 dB at $\theta = -90°$ (270°). The simulation for horizontal polarization shows that there is a value of –10 dB at $\theta = -87.5°$. Using the last measurable values for the extreme near field measurements allows the best correlation to simulation. The last values will be used for the rest of the comparisons unless otherwise stated.

Figure 4.11 illustrates the radiation pattern for the vehicle facing into the plot ($\phi = 90°$). The horizontal polarization, shown in the bottom plot, shows a good consistency between measurement and simulation. The null depth at about $\theta = 45°$ is quite different. The measurement is actually deep (-40 dB) while the simulation is only –10 dB. The vertical plots show a good correlation except that simulation finds a null at $\theta = 80°$ and $\theta = 280°$ while measurement does not show this.

Figures 4.10 and 4.11 show just a few plots of the radiation pattern for the antenna on the vehicle for only one frequency. There are numerous other possible angles and frequencies that a curve could be generated at. Many plots at different angles and frequencies have been examined that are not included to save space. It can be concluded from these plots and Figures 4.9-4.11 that the MM simulated radiation pattern results are very similar to the far field pattern that has been transformed from near field data. There are some errors but it is reasonable to assume that the MM results yield a far field pattern and impedance curve that closely match measurement.

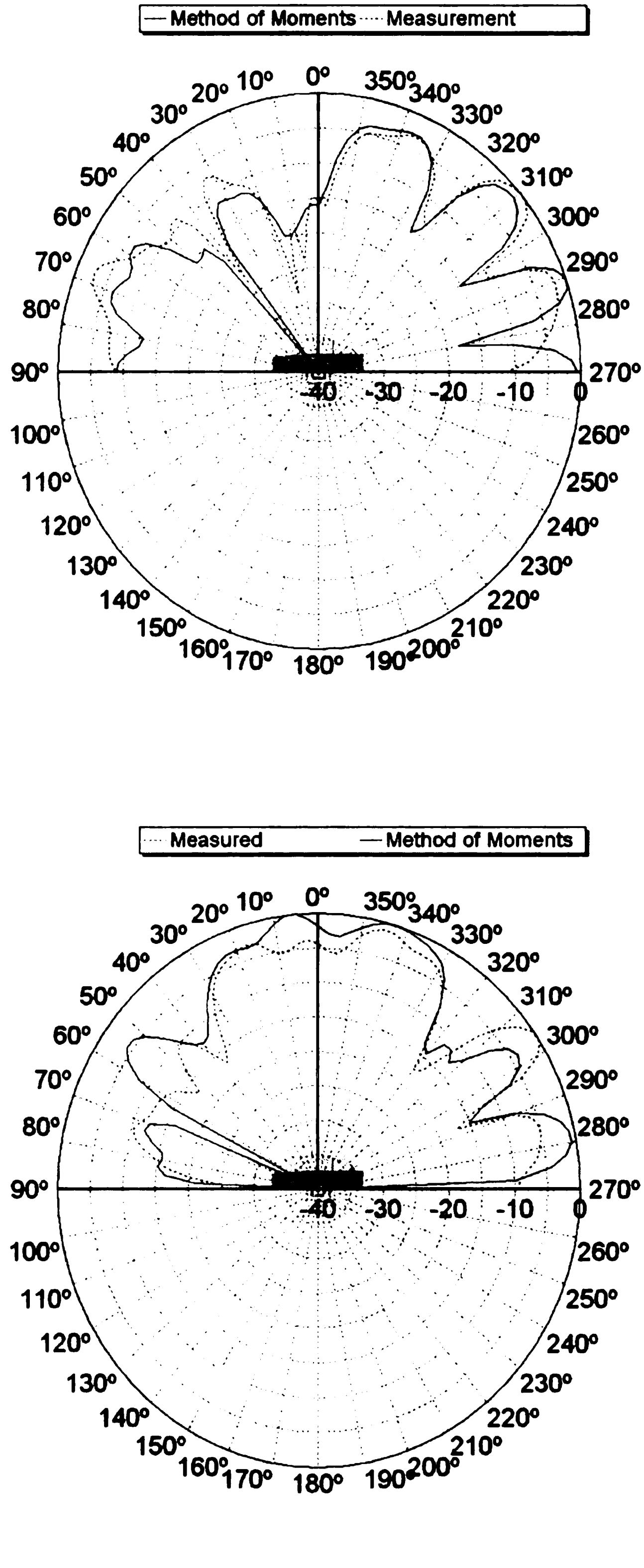

Figure 4.10: Band Own Far Field Transformed from Near Field Measured for Vertical (Top) and Horizontal (Bottom) Polarization Shown with MM Simulation for 350 MHz at $\phi = 0°$ and Vehicle Shown Facing Left (Shown with Normalized Amplitude dB)

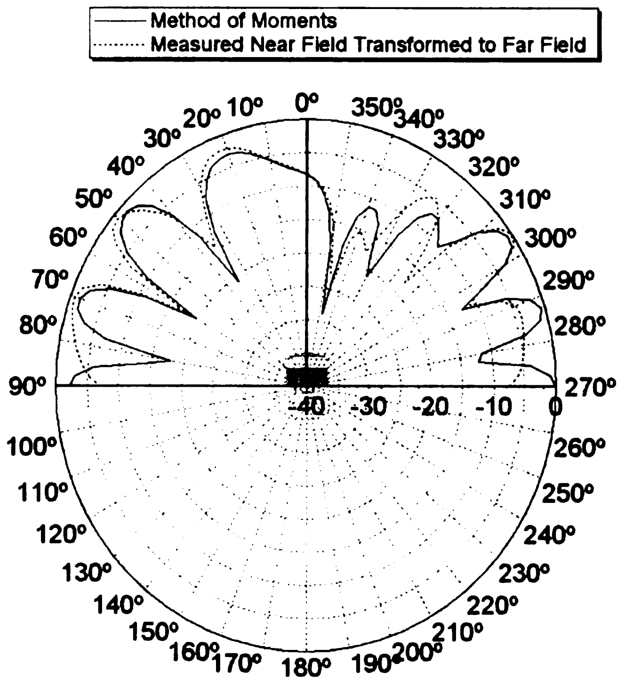

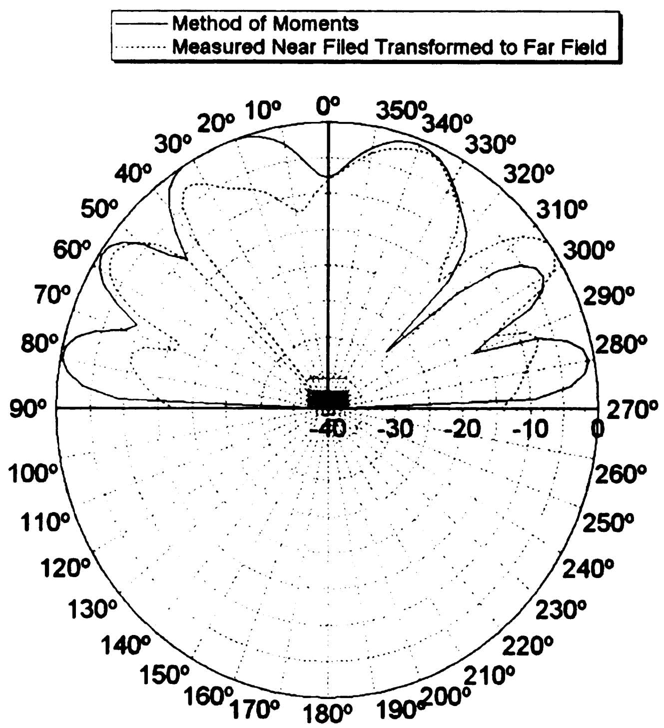

Figure 4.11: Band Own Far Field Transformed from Near Field Measured for Vertical (Top) and Horizontal (Bottom) Polarization Shown with MM Simulation for 350 MHz at $\phi = 90°$ and Vehicle Shown Facing Into the Plot (Shown with Normalized Amplitude dB)

4.3 Comparison of Method of Moments to Measurement and Hybrid Methods

Now that it has been shown that the Method of Moments simulations are usually very close to measurement, hybrid methods can be explored. First, however, an important visual comparison can be made to determine if a hybrid method will yield a good match to a full MM and measured radiation pattern. Looking at the surface currents on the vehicle allows an estimate for how well the radiation pattern will match. This is true because the radiation pattern itself is computed from the surface and line current. There is no way to actually measure the surface current on the vehicle so the MM results are used. This can be justified because the MM radiation pattern is so similar to measurement that the surface currents must also be similar.

Shown in Figure 4.12 is the surface current density for the method of moments simulation for 350 MHz on the test vehicle. The vehicle is oriented with respect to the small axes enclosed in a box in the upper right side of the figure. Looking carefully at this figure, the monopole antenna can be seen on the left rear trunk top. The amount of current on the monopole is indicated by various shades of gray as indicated in the legend on the left side of the figure. This scale is titled "Log Line Cur [A]" and shows the logarithm of the line current on the antenna. This current is usually about the same on all the simulations because the line current always uses the MM. So, the surface current on the vehicle is the most important for comparing simulation results and the line current will not be discussed. The scale titled "Log Surf Cur [A/m]" indicates the amount of surface current on the vehicle itself. The scale goes from the largest at Log (0.0269 A/m) = –1.57 to the smallest at Log (0.00331 A/m) = –2.48. The most surface current density is seen near the antenna on the left rear trunk. The entire left rear corner in fact has the most current density on the entire vehicle. The front part of the vehicle is mostly very dark because there is not much current density there. This is because the rest of the vehicle mostly shadows the front. A large current density can be seen on the pillars and the roof edges. These areas are very crucial since small changes in their geometries can have profound impacts on the resulting current densities all over the vehicle.

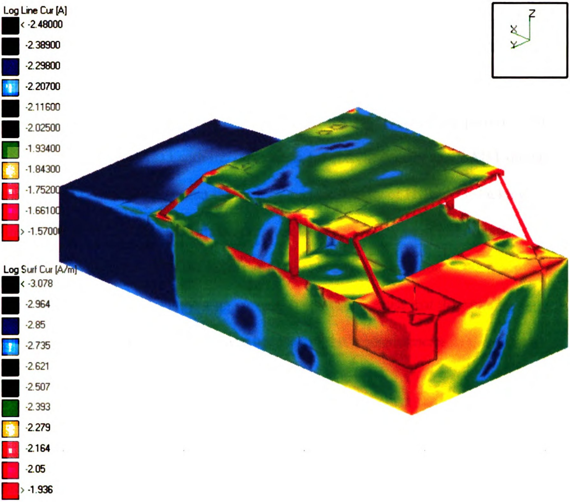

Figure 4.12: The Surface Current Density on the Test Vehicle for the MM Simulation at 350 MHz

4.3.1 Hybrid I

The first hybrid simulation to be compared is "Hybrid I" as described in Chapter 3. This simulation considers a small feed plate on the trunk and the monopole antenna with MM and the rest of the vehicle with PO. This simulation does not include a coupling between the MM and the PO regions. Hybrid I only requires about 100 MB of RAM and 0.20 hours per frequency point. This is about the same computation time as the MM simulation because the segmentation lengths have been reduced to $\frac{\lambda}{15}$. Recall that the MM segmentation length is $\frac{\lambda}{10}$ for the results shown in Figure 4.12. The Hybrid I simulation is a good starting point and will be looked at for 350 MHz.

Figure 4.13 includes the surface current density for Hybrid I (top picture). This is a screen shot from FEKO with the same scale for current density as the MM shown in Figure 4.12. It can be seen that the surface current density of Hybrid I is lacking some of the detail that the MM simulation has. This deficiency most importantly displays a lack of activity on the pillars and the roof edges in addition to the front of the vehicle's edges having almost no current. It can be expected that the radiation pattern may be inaccurate for this curve because of the inconsistencies of the current density.

Figure 4.14 and Figure 4.15 show just two radiation patterns that include both the method of moments simulation and the Hybrid I simulation result. It can be seen that there are some differences between Hybrid I and the MM results for the FFV pattern in the top plot of Figure 4.14. These differences are up to 15 dB in some cases and the general pattern only very loosely follows the MM result. The horizontal case is much different in that major nulls are completely missed by the Hybrid I simulation. Figure 4.15 shows the plots for $\phi = 90°$. The general features of the MM are followed for the vertical polarization plot $0° < \theta < 90°$. However, for $-45°$ (315°) $< \theta < 0°$ neither the features nor the amplitudes of the patterns match very closely. Many other cuts have been examined for Hybrid I and the results are similar.

Hybrid I and Hybrid II have extremely similar impedance plots. These are shown in Figure 4.16 (only Hybrid II is shown). The impedance curves have the same general shape but the Hybrid I-II curve is larger in "radius" than the measured and MM curves. The impedance is one of the most important parameters of the antenna and it is imperative to make a reasonable correlation between simulation and measurement. Hybrid I is thus insufficient to properly model the vehicle surface current, input impedance and the far field radiation pattern.

4.3.2 Hybrid II

Hybrid II is a very similar simulation to Hybrid I except that the coupling between the MM and the PO region is considered. This has a significant impact on the RAM consumption and computation time. For this simulation, roughly 800 MB and 0.24 hours per frequency point are required. The bottom plot of Figure 4.13 shows the surface current density for 350 MHz. There are clearly some major differences between the bottom plot on Figure 4.13 and the current shown on Figure 4.12 by the MM. In Figure 4.13 many parts of the vehicle do not show a high enough current density. This is especially true on the roof and sides of the vehicle. It appears that the area around the MM feed plate may be properly modeled but the surrounding areas are grossly incorrect.

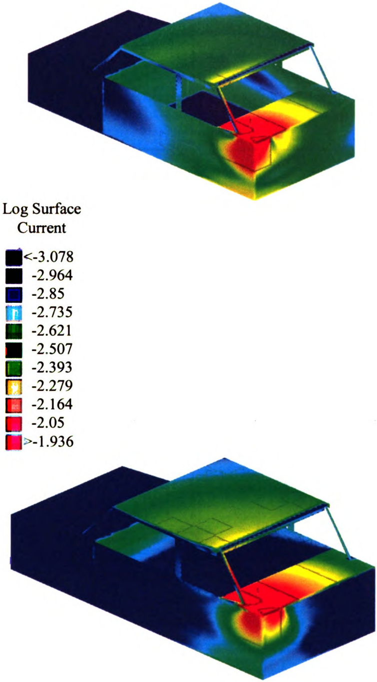

Figure 4.13: Hybrid I (top) and Hybrid II (bottom) Surface Current Density for 350 MHz

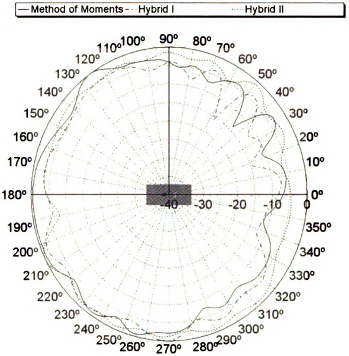

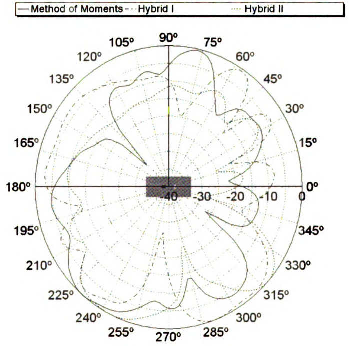

Figure 4.14: Band Own Far Field MM, Hybrid I and Hybrid II Simulation for Vertical (Top) and Horizontal (Bottom) Polarization for 350 MHz at $\theta = 85°$ and Vehicle Facing 0° (Shown with Normalized Amplitude dB)

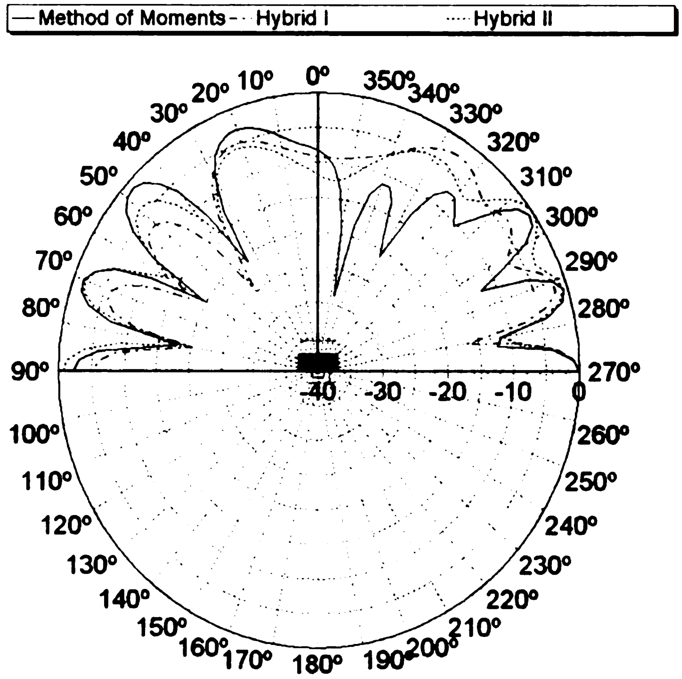

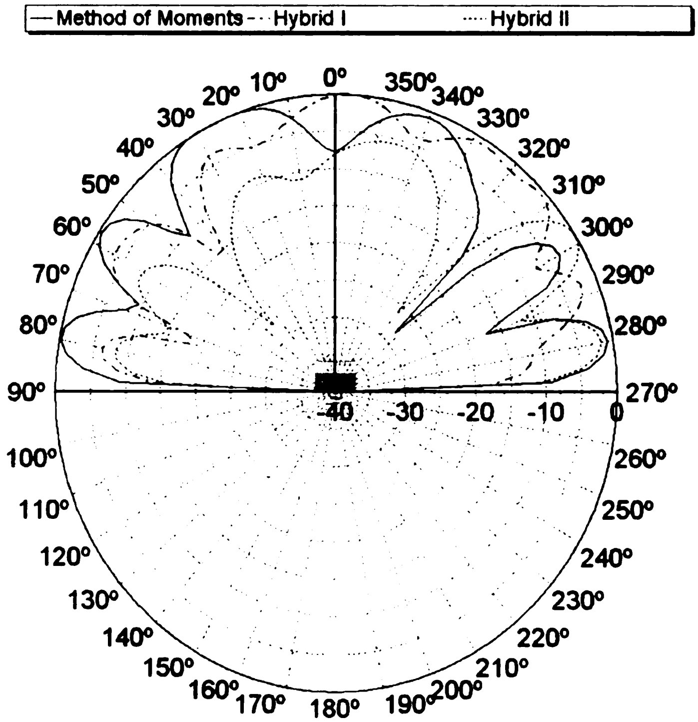

Figure 4.15: Band Own Far Field MM, Hybrid I and Hybrid II Simulation for Vertical (Top) and Horizontal (Bottom) Polarization for 350 MHz at $\phi = 90°$ and Vehicle Shown Facing Into the Plot (Shown with Normalized Amplitude dB)

Figure 4.14 shows that for the vertical polarization, the Hybrid II simulation is mostly similar to the Hybrid I simulation. No significant improvements from Hybrid I can be seen. For the horizontal polarization, the Hybrid II plots show only some correlation to the MM region. There may be some small improvements here in that the overall amplitudes appear to better match the MM. The largest inaccuracy of Hybrid II is the null at 135°. This null is not found in the simulation with Hybrid II but is in the MM results. Figure 4.15 illustrates some improvements for Hybrid II. For the vertical polarization (top plot) there is a better correlation to MM than Hybrid I. This is especially true for angles 315° to 270° (-45° to –90°). In the horizontal polarization plot in the bottom picture in Figure 4.15, there are some distinct improvements with Hybrid II. The null at $\theta = 315°$ (-45°) in simulation is found with Hybrid II but not with Hybrid I. Overall, the Hybrid II curve is closer to MM than Hybrid I. Additionally, the impedance plot of Hybrid II is shown in Figure 4.16. This plot shows an inconsistency between measurement and simulation as discussed earlier with Hybrid I. Many other plots of Hybrid II have been compared to the MM solution and they appear to be similarly slightly inaccurate despite the marginal improvements from Hybrid I.

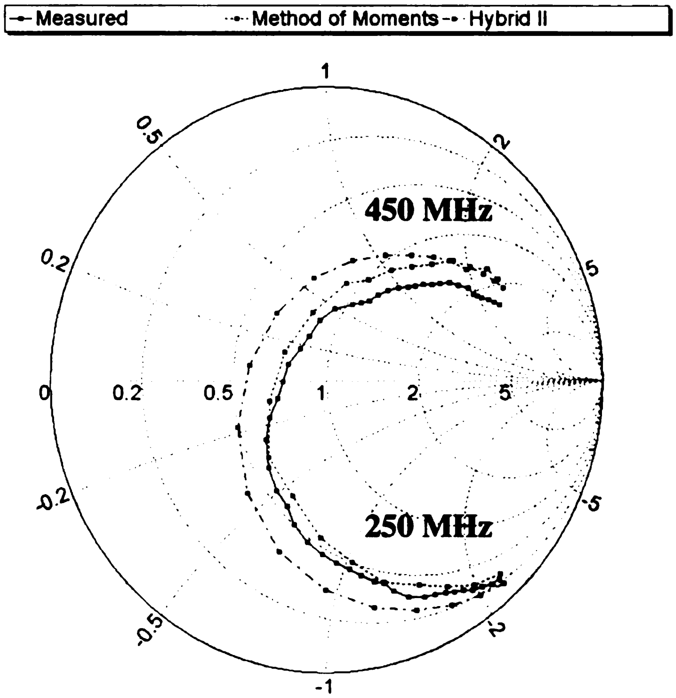

Figure 4.16: The Impedance Curves for Measurement, MM and Hybrid II for Band Own 250-450 MHz

4.3.3 Hybrid III

The simulation for Hybrid III is devised largely as an experiment of interest. The impedance plot for Hybrid II is nearly the same as Hybrid I. So, only Hybrid II is shown in Figure 4.16. It is clear that there are some differences between the Hybrid curve and the measured and simulated with MM. The Hybrid III simulation has been developed to try and match the impedance better for the 250-450 MHz range and see how the current flows on the ground. An attempt has been made to model the ground of the radome as discussed in Chapter 3. The ground is modeled as a 10.2 m radius circular disc and is considered with PO. This simulation, however, has too many unknowns (roughly 220,000) to solve for the impedance at multiple frequency points so no results are shown for Hybrid III. It is expected that this will not largely affect the input impedance anyway since the MM feed plate at the antenna feed location is largely responsible for this aspect of the simulation. This is because impedance is the ratio of the excitation voltage to the current at the feed location that is considered by the accurate MM.

4.3.4 Hybrid IV

It can be seen from Hybrid I and Hybrid II that the surface current densities on the vehicle are not close enough to the MM solution to allow a very good correlation between their radiation patterns. There is an especially large discrepancy on the pillars and roof edges. These areas are insufficiently modeled with PO and should be considered with MM. Considering these areas with MM will increase the computational cost of the solution. This is necessary, however, since Hybrid I and Hybrid II are simply too inaccurate for certain angles. Considering the edges and pillars with MM and the rest of the body with PO, as illustrated in Figure 3.8, yields some interesting results. This simulation requires 6576 MB of RAM and about 10 hours per point. This is a significant increase in computation time and RAM from both Hybrid I and Hybrid II.

The surface current density on the vehicle is shown in the top image in Figure 4.17. Looking at this picture, and comparing it to Figure 4.12, it can be seen that there are some improvements from Hybrid I and Hybrid II. The surface current density on Hybrid IV in Figure 4.17 depicts more current activity on the pillars and roof region than Hybrid I and II. Hybrid IV also shows a fairly good correlation for the rear trunk surface current. This is just a preliminary comparison to see if the hybrid simulation has modeled the surface currents roughly as well as the MM simulation. There are still some differences but this will hopefully allow a more accurate radiation pattern.

Though the Hybrid IV surface current densities appear to be more similar to the MM simulation than Hybrid I and Hybrid II, the radiation patterns are the most important comparison. It may be useful to additionally reference Figure 4.14 for this part of the discussion. Figure 4.18 shows a comparison between the MM simulated and Hybrid IV results for $\theta = 85°$ for both vertical and horizontal polarizations. Hybrid V is also included in these plots and will be discussed in the next section. The Hybrid IV simulation for vertical polarization is depicted in the top part of the figure. There is a very good correlation between MM and Hybrid IV for the angles $-90°$ ($270°$) $< \phi < 15°$. This is much more accurate than Hybrid II especially since the amplitudes and general features of the curve are not included with Hybrid II.

For the horizontal plot, shown in the bottom plot of Figure 4.18, it is very difficult to determine if Hybrid IV shows improvement since there is little correlation to the MM simulation. Hybrid IV shows two additional nulls in the area $255° < \phi < 315°$ for a total of three nulls. The MM and Hybrid II curves show only a single null. Realistically, however, this curve is mostly inconclusive. The $\theta = 85°$ plots for horizontal polarizations typically show the worst correlation between curves. This is probably because the extreme low elevation angles represent a wave encountering the lowest part of a side of the vehicle with the polarization orthogonal to the receiving monopole. The received signal strength is thus due mostly to reflections and coupling that are difficult to model with the PO approximation.

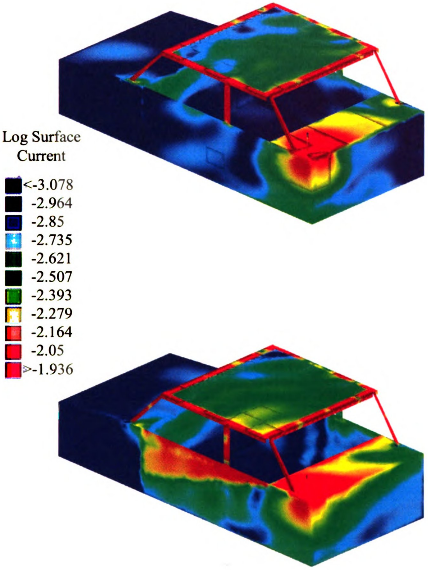

Figure 4.17: Hybrid IV (Top) and Hybrid V (Bottom) Surface Current Density for 350 MHz

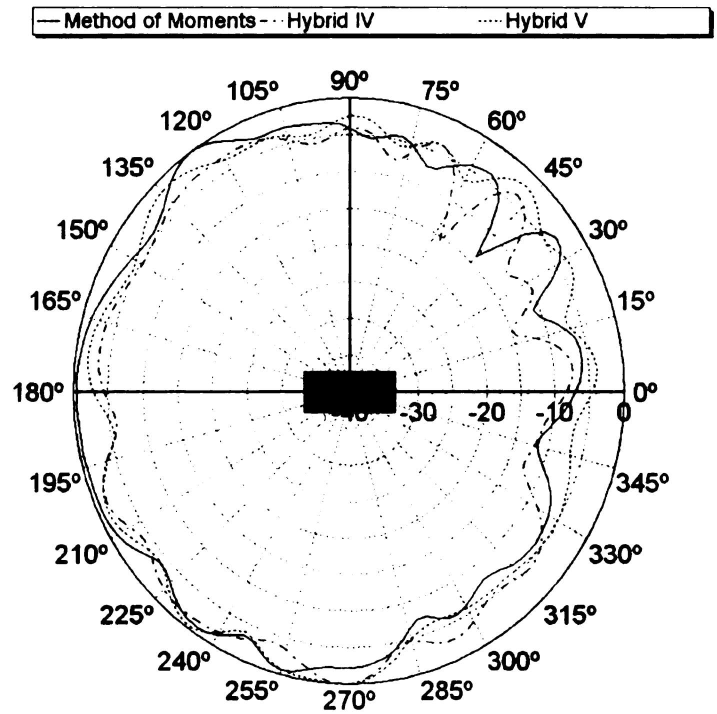

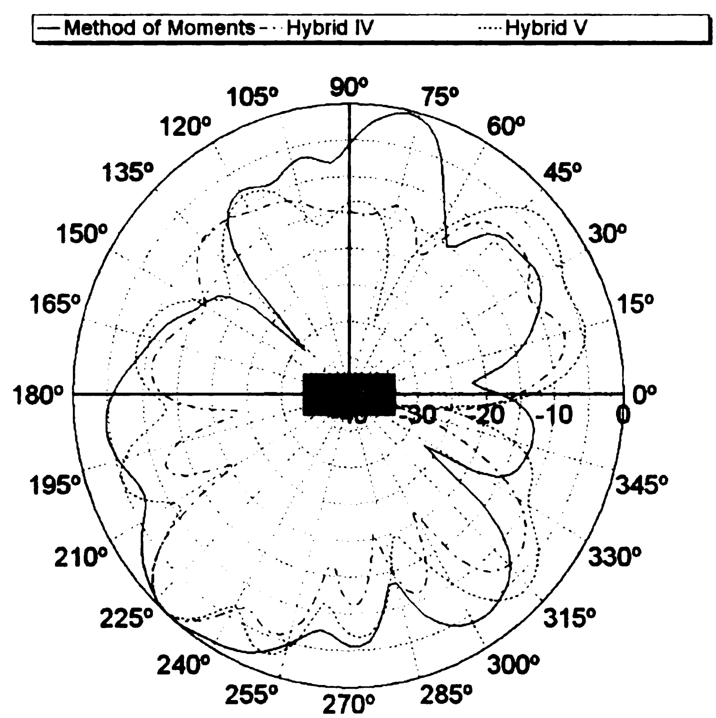

Figure 4.18: Band Own Far Field MM, Hybrid IV and Hybrid V Simulation for Vertical (Top) and Horizontal (Bottom) Polarization for 350 MHz at $\theta = 85°$ and Vehicle Facing 0° (Shown with Normalized Amplitude dB)

Figure 4.19 depicts vertical and horizontal plots for $\phi = 90°$. The vehicle is shown facing into the plots. The null depths at 60° and 45° are more accurate than Hybrid II. There is also more distinct detail for the angles 320° (-40°) $< \theta <$ 290° (-70°). The null depths at ± 80° are much too deep using Hybrid IV, but generally it could be concluded that Hybrid IV is more accurate for this cut.

The horizontal polarization plot, depicted in the bottom image in Figure 4.19, shows some improvement over the previous hybrid approaches. The overall amplitude of the curve is more consistent with the MM simulation. There is not a significant improvement for this angle, however, considering the increase in computational cost for Hybrid IV.

Since Hybrid IV has shown some improvements over the previous simulations, an additional cut will be looked at here. Figure 4.20 depicts horizontal and vertical patterns for $\phi = 0°$ at 350 MHz. The vehicle is shown facing to the left. From the angles –90° (270°) $< \theta <$ -50° (310°) there is an excellent correlation between the MM and Hybrid IV. This is probably because those angles are accurately simulated with the MM since that area faces the rear trunk that has the MM feed plate. On the other side of the vehicle, the null depth at about θ =40° is not as deep as the MM simulation. However, this is actually closer to the measured null depth as shown in Figure 4.10. The only other significant inaccuracy is the large beam amplitude at θ =25°. The MM simulation has amplitude of –12 dB while Hybrid IV computes the amplitude to be about –5 dB. Overall, the vertical polarization Hybrid IV compares quite well with MM simulation.

The horizontal polarization plot, shown in the bottom of Figure 4.20, depicts the Hybrid IV curve loosely following the MM curve. There is a fairly large discrepancy at the angle $\theta = -35°$ (325°). Hybrid IV computes a null there (-40 dB) while the MM simulation computes only a depth of around –12 dB. Also, at approximately $\theta = 5°$ there is a beam height of 0 dB in MM but a null in Hybrid IV of nearly –7 dB. At $\theta = 65°$ the MM simulation finds a null depth of –40 dB. Hybrid IV computes a depth of –25 dB at approximately the same location ($\theta = 70°$). Hybrid IV compares quite well with the MM simulation for the horizontal polarization in addition to the vertical polarization.

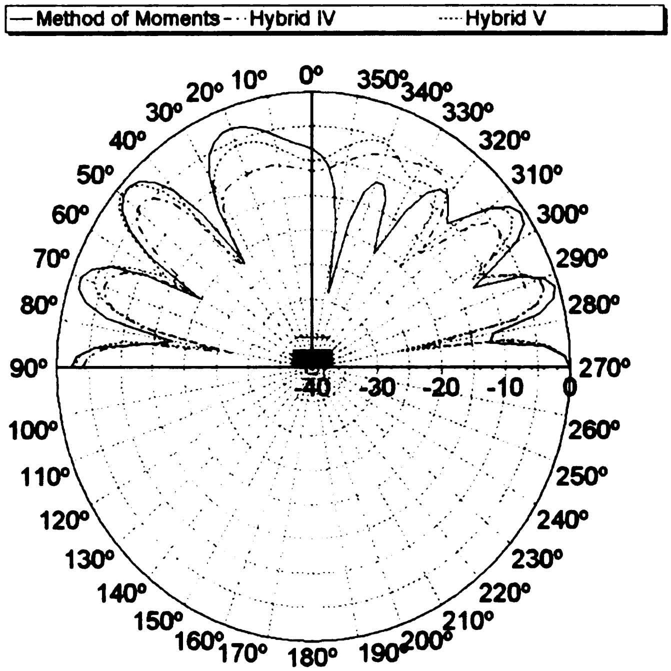

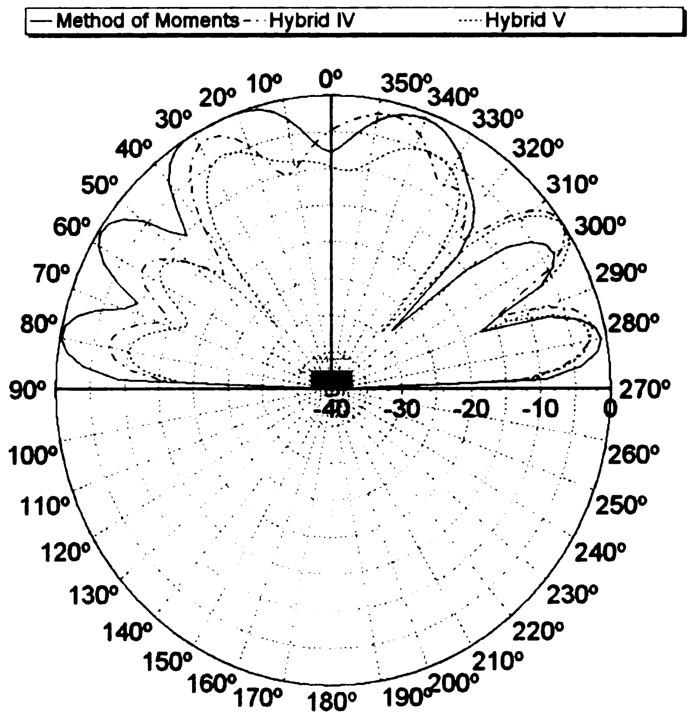

Figure 4.19: Band Own Far Field MM, Hybrid IV and Hybrid V Simulation for Vertical (Top) and Horizontal (Bottom) Polarization for 350 MHz at $\phi = 90°$ and Vehicle Shown Facing into the Plot (Shown with Normalized Amplitude dB)

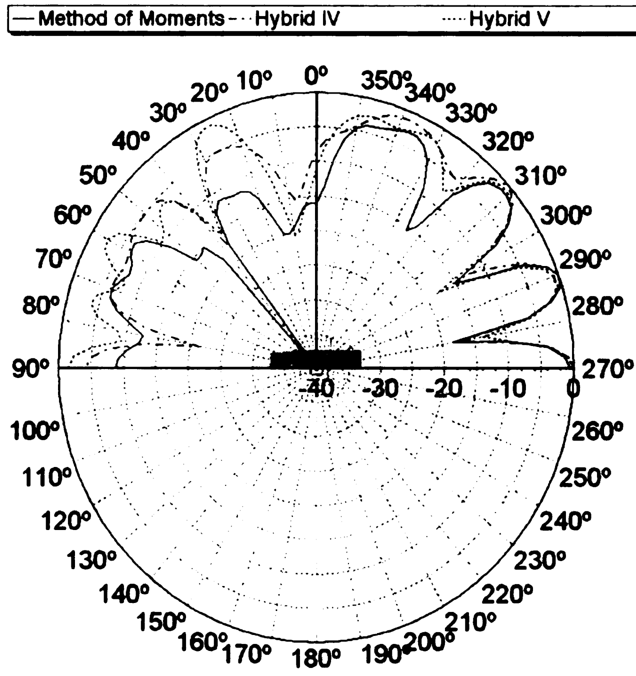

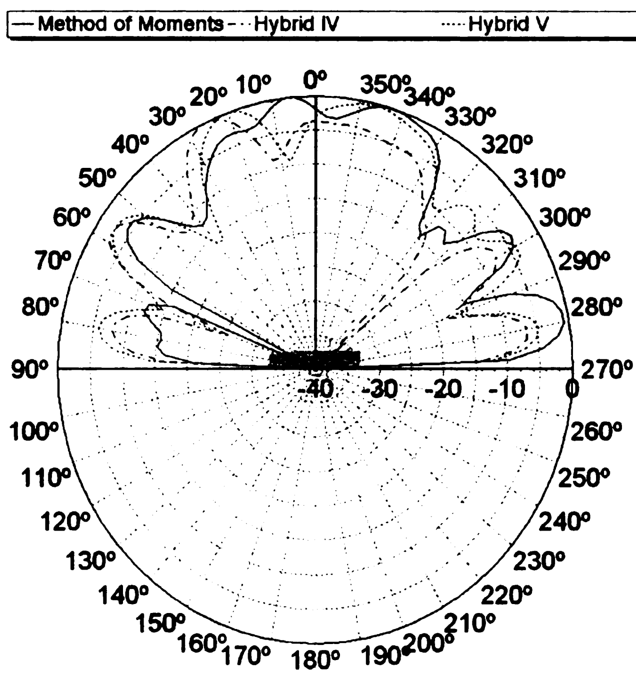

Figure 4.20: Band Own Far Field MM, Hybrid IV and Hybrid V Simulation for Vertical (Top) and Horizontal (Bottom) Polarization for 350 MHz at $\phi = 0°$ and Vehicle Shown Facing to the Left (Shown with Normalized Amplitude dB)

4.3.5 Hybrid V

The Hybrid V simulation is the most advanced hybrid simulation developed in this study. This simulation, as discussed in Chapter 3, implements FEKO's correction cards for edge currents on plates. The same areas are considered with PO and MM on the vehicle. The PO areas use the correction cards to account for fringe wave currents. Since most of the vehicle is still considered with PO, using this correction on all edges could allow a significant improvement in the surface current density and ultimately the radiation pattern. Figure 4.21 shows the full MM surface current density for the driver side panel of the vehicle (left side) alone. The rest of the vehicle is not included in this simulation. The monopole antenna is included with the feed plate that is also considered with MM. The feed plate and monopole are difficult to see in the image since they are directly behind the side panel. The surface current density can be seen to be changing a lot over the entire area of the panel. There is plenty of detail on the top edge of the panel where current density is changing along the edge.

The top picture in Figure 4.22 shows the exact same side panel with the monopole antenna and feed plate. In this figure, the side panel is considered with PO as in Hybrid I through Hybrid IV. There is no correction for the top edge. It can be seen that the top edge is not very similar to the MM density picture in Figure 4.21. The bottom picture in Figure 4.22 shows the exact same panel as Figure 4.21 but the correction on the top edge is included. This not only makes the current density around the top edge similar to the MM but also corrects the currents in the middle of the panel as well. All the edges of the vehicle that don't form a corner are corrected in Hybrid V.

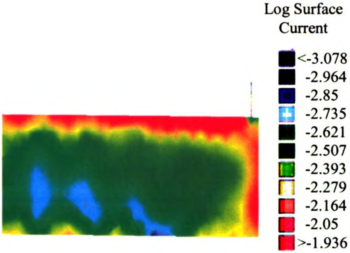

Figure 4.21: Surface Current Density on Side Panel of Vehicle and Monopole Antenna with Feed Plate all Considered with the Method of Moments

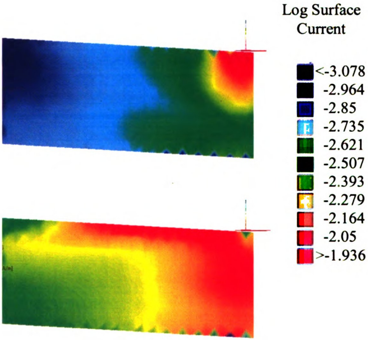

Figure 4.22: The Surface Current on the Side Panel of the Vehicle Considered with PO (Top) with No Edge Correction and (Bottom) with Edge Correction on the Top Edge

The plates that form a corner use a separate wedge correction feature that corrects the surface current density on both sides of the wedge. A wedge correction is implemented at all locations where is a wedge on the vehicle formed by combining two plates. This will hopefully improve the radiation pattern since the current density on the surface of the vehicle should be drastically improved.

The surface current density on the vehicle for Hybrid V is shown in the bottom image of Figure 4.17. Comparing this to the full MM surface current density in Figure 4.12 reveals that there are some improvements over Hybrid IV. First of all, the rear trunk and rear "bumper" have a much higher current density in Hybrid V. This is more consistent with the MM simulation. Also, the base of the front left pillar is more illuminated than Hybrid IV. This is more consistent with MM. Many edges show a slight improvement over Hybrid IV and appear more like the MM simulation. This should lead to some improvements in the accuracy of the radiation pattern. Implementing these many corrections to the wedges and edges of the vehicle have no impact on the required RAM. In fact the required RAM is the same as Hybrid IV. However, since there are additional computations the total time is increased by 30% to a total of approximately 13 hours per frequency point.

The resulting radiation patterns are compared with Hybrid IV in the previous figures. The top image in Figure 4.18 shows the vertical polarization for $\theta = 85°$ for the MM, Hybrid IV and Hybrid V. Hybrid V has no noticeable improvements over Hybrid IV in this cut. In fact Hybrid V completely misses the null at $\phi = 45°$. This cut is probably mostly similar in accuracy to Hybrid IV. The bottom image in Figure 4.17 for the horizontal polarization at 350 MHz shows some improvement over Hybrid IV.

This is indicated for angles 255° < ϕ < 315° since the nulls are more closely matched. There are also some improvements in the area of 115° < ϕ < 210° where the amplitudes more closely match MM. This is probably because for low elevation angles, with the incorrect polarization, reflections are important. The induced currents on the vehicle are critical when considering reflections and are more closely modeled when corrections are used in Hybrid V.

The vertical polarization results for ϕ = 90° are depicted in the top image in Figure 4.19. The vehicle is shown facing into the plot. For this cut there are certainly some improvements over Hybrid IV. This is evident for all the angles to the left of the vehicle 0° < θ < 90° where there is a much better correlation to the MM simulation. The amplitudes and null locations match very well. For the angles –45° (315°) < θ < 0°, both Hybrid IV and Hybrid V fail to accurately represent the pattern. However, for the remaining angles Hybrid V is slightly superior to Hybrid IV in accuracy. The horizontal plot is in the bottom of Figure 4.19. Here, it can be seen that the null at θ = 315° is well captured in Hybrid V. The angles 0° < θ < 90° show a better following of the MM features but the amplitudes of Hybrid IV are closer to the MM simulation. It is evident that Hybrid V, despite the slight inaccuracies in the horizontal plot is generally more accurate than Hybrid IV for this cut.

The vertical polarization results for ϕ = 0° are depicted in the top image in Figure 4.20. The vehicle is shown facing to the left. For this cut there are some improvements over Hybrid IV. For the angles -90° (270°) < θ < 0° Hybrid V is somewhat more accurate than Hybrid IV. For the angle θ = 10° the null depth is more accurate with Hybrid V than Hybrid IV. However, the beam amplitude at θ = 25° is less accurate. There is slightly more detail in the remaining angles but the correlation to MM is not significantly better. The horizontal polarization shown in the bottom image of Figure 4.20 illustrates that there is one major improvement in that the erroneous null simulated by Hybrid IV at $\theta = 315°$ is no longer existent. In fact, that angle now shows the proper beams and nulls that are found in the MM solution. Hybrid V shares with Hybrid IV the same minor error at $\theta = 10°$ of simulating a null. The remaining curve follows the MM solution fairly well without many significant errors.

It is shown in Figures 4.18 through 4.20 that the overall performance of Hybrid V is superior to Hybrid IV. Of course, there are several other cuts that can be explored. After looking at many other angles, it can be concluded that there is a general trend of Hybrid V being more accurate for some angles. Hybrid V is usually not less accurate than Hybrid IV as is evident in looking at just three cuts at both polarizations. It can thus be concluded that overall, Hybrid V is the most accurate simulation model developed for the test vehicle. Its current density shows the best correlation to the MM simulation and the radiation patterns are very close indeed. The input impedance has been simulated for only three frequency points and does not generate a smooth curve. This is because of the high computation cost of Hybrid V. However, it is expected that the impedance looks at least as good as the Hybrid II impedance curve in Figure 4.16 if not better. This is because Hybrid V has more MM regions and should have an overall accurate representation of the full MM surface current density. Also, Hybrid V uses the same MM feed plate as Hybrid II and since the impedance is the ratio of the excitation voltage to the current at that location it is reasonable to guess that the impedance curves are similar. All three simulated points with Hybrid V are very near points on the Hybrid II impedance curve. This shows that Hybrid V is a reasonably good means for approximating the computationally expensive MM simulation.

CHAPTER 5

CONCLUSIONS

5.1 Overview

As vehicles begin to require a larger number of antennas operating at higher frequencies, the shape of the vehicle itself impacts the optimum design and location of these antennas. For frequencies greater than 1 GHz the challenge for automotive antenna engineers is to first design the antenna in free space. Then, the correct location on the vehicle to mount the antenna must be determined. Engineers then need to take numerous measurements to ensure that the antenna on the vehicle is performing within specification. The antenna design may need to be changed along with the location in order to meet the rigorous specifications of, for instance, satellite radio. This poses a significant problem to engineers as they attempt to reduce design cost and cycle time. For this reason, simulation is looked at as a means to decrease the need for expensive measurements. The proper simulation technique needs to be applied to achieve a reasonable result. The results of the simulation need to be verified with comparison to measurement to ensure simulation is a viable means to make design decisions.

A model of an automobile has been constructed with wood, metal and fine brass mesh. This model is fairly representative of a small vehicle and has a length of 3.6 m, a height of about 1.5 m and a width of 1.8 m. This vehicle has been constructed because it is easier to model in simulation than an actual automobile that has discontinuities, a variety of materials, and smooth curves. This physical model is composed of simple geometrical shapes that have made it easy to model in simulation.

Having an actual test vehicle and a simulation model with exactly the same dimensions allows a thorough comparison between measurement and simulation. The measured and simulated ranges of frequencies have been discussed and begin at 70 MHz and end at 1 GHz. This range of frequencies includes the previously discussed band FM, band 3, band Own, band 4-5, and band GSM. The choice of test antenna is a quarter wavelength monopole.

The method of moments technique is an accurate, but computationally expensive, means for simulating the radiation pattern of an antenna on the vehicle. Band 4-5 and band GSM can't be accurately simulated with the MM due to the large RAM requirements. Hybrid methods have been explored as a possible remedy for this while maintaining reasonable accuracy. These simulations have been compared to measurement in Chapter 4.

5.2 MM simulation

The method of moments technique is explained in Chapter 3. The simulations for Band FM, Band 3 and Band Own have been run with a $\frac{\lambda}{10}$ maximum segmentation length in FEKO. Band 4-5 is run with a maximum segmentation of $\frac{\lambda}{5}$ and Band GSM has segmentation lengths even greater than $\frac{\lambda}{5}$ so that the simulation can fit in the available 16 GB of RAM. This is beyond the bounds of acceptable segmentation lengths as specified by the software package FEKO as discussed in Chapter 3. The results for these simulations are considered inaccurate.

Chapter 4 discussed the comparison between the impedance measurement and simulation. An excellent correlation is made for Band FM, Band 3, and Band Own. Simulation is shown to nearly match measurement for these bands. Band GSM and Band 4-5 did not show the correct results for impedance, but the general features of the impedance curves are consistent. The far field patterns for Band FM, Band 3, and Band own also show an excellent match to measurement. It has been concluded, due to the closeness of measurement and simulation for the impedance and far field radiation patterns, that the method of moments simulations are quite close to measurement.

Table 5.1 shows the number of metallic edges in simulation with a $\frac{\lambda}{10}$ maximum segmentation length. This includes the estimated time requirement if the simulation could actually run for Band 4-5 and Band GSM. The time per frequency point of the simulation is related to the frequency raised to the third power. The time for Band 4-5 is estimated to be roughly 30 hours per frequency point. The computation time per frequency point is about 90 hours for Band GSM.

Band (MHz)	**Number of Metallic Edges (MM) with λ/10 Maximum Segmentation Length**	**RAM Required (MB)**	**Average Simulation Time per frequency point (hours)**
FM (70 - 120)	3972	258.150	0.0019
3 (175 - 235)	11256	1,961.420	0.0196
Own (250 - 450)	25882	10,373.720	3.0758
4-5 (670 - 870)	83786	112,042	≈ 30
GSM (800 - 1000)	105706	178,818	≈ 90

Table 5.1: The method of moments computational requirements for all studied frequency bands

As can be seen in Table 5.1, there is a large computational cost associated with the required RAM. Additionally, the estimated simulation time per frequency point is fairly large for Band 4-5 and Band GSM. This would require a long simulation time if multiple frequency points are needed. This makes the method of moments the most accurate of all the simulations studied here but also the most expensive in terms of storage space.

5.3 Hybrid Simulations

The hybrid methods discussed in Chapter 3 are one possible way to find results at a reduced computational cost. Tabulated in Table 5.2 are the computational requirements for Hybrid I through Hybrid V for Band Own only. This band is used only because it is the highest frequency that can be completely simulated with the accurate method of moments. Additionally, the center frequency of 350 MHz is most often used.

Hybrid For Band Own 350 MHz	Maximum Segmentation Length	Number of Unknowns MM	Number of Unknowns PO	RAM (MB)	Average Simulation Time per frequency point (hours)
I	λ/15	94	53362	101.236	0.208
II	λ/15	94	53362	798.225	0.241
III	Ground λ/5 Vehicle λ/15	94	222400	3592.506	-
IV	λ/10	1954	23954	6576.008	10.02
V	λ/10	1954	23954	6576.008	13.10

Table 5.2: The computational requirements for the hybrid simulations

The results from these simulations are compared for some typical cuts to the MM solutions in Chapter 4. Hybrid I through Hybrid III all use a maximum segmentation length of $\lambda/15$. This is because the RAM requirements for a $\lambda/10$ simulation are so low that a smaller segmentation length is used to try to maintain a good accuracy. Hybrid I considers the entire vehicle with PO and the monopole with the small feed plate just below the monopole antenna on the left rear trunk top with MM. The results from Hybrid I show in Chapter 4 that the accuracy of the radiation pattern is quite different from the MM simulation.

Hybrid II has the same maximum segmentation length and thus has the same number of PO and MM unknowns. The RAM required is larger (798.225 MB) because a coupling between the MM regions and PO regions is now considered. There is an increase in computation time related to this increase in RAM: Hybrid II takes 0.241 hours to complete. Hybrid II is shown in Chapter 4 to also be deficient in accurately capturing the correct radiation plot. Additionally, the impedance plot of Hybrid II is slightly shifted from the MM and measured curves.

Hybrid III has a finite circular ground plane that is considered with PO instead of as an infinite PEC. This model attempts to simulate the condition in the radome since the radome has a finite ground plane. However, this simulation has too many unknowns to solve. Also, it is very difficult to estimate the computation time per frequency point. This is because the ground plane uses a maximum segment length of $\lambda/5$ and the vehicle uses $\lambda/15$. It can be assumed that the computation time is much greater than 20 hours per frequency point.

Hybrid IV considers the roof edges, all four pillars, the feed plate, and monopole antenna with MM and the rest of the vehicle with PO. Since Hybrid II shows better results than Hybrid I, the coupling between the PO and MM regions is considered. This simulation is run because the radiation patterns resulting from Hybrid II and I are too inaccurate to draw any certain conclusions about the antenna performance on the vehicle. Many null depths are inaccurate and occasionally, as described in Chapter 4, the general shape of the radiation pattern is not correct. As the amount of area containing MM regions increases, the computational cost increases also. The RAM required is 6,576 MB and requires 10 hours per frequency point to complete. From the MM solution in Table 5.1, this is a 64 % savings in RAM but a 325% increase in computation time. The simulation represents a possible solution for a computing system that has only half the available RAM but three times the computing power. This simulation should run well on a system with 8 GB of RAM and with two 3 GHz processors. This solution could possibly be computed with a PC cluster with only two machines with modern computing abilities. The accuracy of this simulation is still lacking for some cuts. The surface current density on the test vehicle does not match the density from the MM simulation as shown in Chapter 4. Since the surface current is integrated to find the far field values, an improvement of the surface current density will impact the radiation patterns. For this reason, the simulation model Hybrid V is developed.

Hybrid V incorporates exactly the same geometry as Hybrid IV. Again, the roof edges, pillars, monopole antenna, and feed plate are all considered with the method of moments. The rest of the vehicle is considered with PO. For this simulation, special correction calculations are performed on the boundaries of PO regions. These corrections are aimed at improving the surface current density accuracy. This will ideally improve the far field radiation pattern. Since the geometry is the same as Hybrid IV, the RAM required is also 6576.008 MB. The computation time is slightly larger however due to the increase in calculations. The computation time of 13 hours per frequency point represents a 433% increase in the calculation time. This is a significantly longer time than the MM solution but represents a 64% savings in RAM. Hybrid V is the most advanced simulation model developed in this study. The accuracy of the solution is discussed in Chapter 4 and is slightly better than Hybrid IV. The surface current has shown some definite improvements over Hybrid IV. Additionally, many cuts show a better correlation to the MM simulation. There are still some details in the general pattern shapes that are left out in Hybrid V however. These discrepancies could be reduced by further increasing the areas considered with MM. This will increase the accuracy of the solution. However, this will also further increase the computational cost of the solution and defeat the purpose of exploring hybrid methods, which is to reduce the computational cost and allow high frequency simulations.

5.4 Simulation of an Antenna on a Vehicle

The overall goal of this study is to allow the simulation of high frequency antennas on vehicles. It has been shown that for the available computing resources the method of moments simulations cannot be run for frequencies greater than Band Own (250 – 450 MHz). This necessitates the use of hybrid methods. Though there are a variety of hybrid methods one could apply, the PO with MM method has been explored here. These hybrid methods are used only for Band Own since it is the highest frequency for which a full MM simulation can be run. From this study, a general algorithm could be applied to set up a simulation using the hybrid PO - MM method.

First, a simulation model of the vehicle needs to be constructed in FEKO. Importing a CAD drawing of the vehicle can accomplish this. Once the three dimensional CAD drawing is imported into FEKO, a triangular mesh can be applied to the vehicle. The mesh should obey the segmentation and triangular criteria as specified by FEKO. A $\lambda/10$ maximum segmentation length of an edge on the triangle is typically sufficient.

If possible, a full MM simulation of the vehicle needs to be run. A full simulation of the vehicle with the method of moments will allow a very accurate solution for the radiation pattern and input impedance. Also, the surface currents on the vehicle will be accurately simulated with the MM. Once this simulation is complete, the vehicle should have a new mesh created that has a variable segmentation length. Areas that have a very low surface current density can have a larger triangle segment length so as to save in RAM consumption. Surface areas near the antenna feed point, at high current density locations or at discontinuities should maintain the $\lambda/10$ maximum segmentation length. Once this is complete, the model can be further modified to have some areas considered with PO and others with MM. Flat areas that have low current activity away from the feed location are best considered with PO. Full ray tracing should always be performed. This requires additional computational time but is essential to maintain any accuracy. Coupling between the MM regions and PO regions should certainly be considered. This is proven through an increase in accuracy in Hybrid II over Hybrid I. Corrective wedges, as applied in Hybrid V are unlikely to be applicable to an actual vehicle model. This is because most actual vehicle models don't have sharp corners formed by the intersection of large planes like the test vehicle in this study. The application of the corrective edges in FEKO could, however be applied in some cases depending on the location of the PO and MM regions.

Once the PO region is applied, the hybrid simulation should be compared with the full MM simulation to ensure it maintains the desired level of accuracy. Some additional modification could be necessary if the hybrid simulation accuracy is unacceptable. The PO hybrid model should represent a significant savings in the RAM requirements. However, it may also require a larger computation time. It is therefore recommended that this model be applied to computer systems that have faster processing and RAM bus speed with less RAM.

5.5 Conclusions

In this thesis, an advanced antenna measurement facility is presented. This measurement facility allows the three-dimensional far field radiation pattern of an antenna mounted on a vehicle to be measured. With use of this facility, measurements are performed on many frequency bands ranging from 70 MHz to 1 GHz on a test vehicle with a quarter wavelength monopole. Simulation is also a very important means for engineers to make design decisions about the antenna on the vehicle. The test vehicle is modeled in FEKO, a MM based software package, and is simulated for the various bands. Frequencies greater than 450 MHz, however, require too many computational resources for an accurate simulation. For this reason hybrid methods are discussed. These hybrid methods are developed for the center frequency of 350 MHz of Band Own. A variety of methods are explored and ultimately Hybrid V yields the best results. This method features a 64% savings in RAM but a 425% increase in computation time. Though the entire simulation is not run for other frequency bands, using Hybrid V allows Band 4-5 (670 MHz to 870 MHz) to run with only 7,860 MB as opposed to the MM requirement of 112,042 MB. This is a 90% reduction in RAM. Though there will be a longer run time, at least this simulation can now be run with the available resources. Hybrid V allows Band GSM (800 to 1000 MHz) to run with 11,360 MB instead of the 178,818 MB required by the full MM. This is also a 90% reduction in RAM requirements. For faster computers with less available RAM, new antenna ideas can be explored in simulation without taking the time to build numerous prototypes and measure the antenna on the automobile. Once a design concept is functioning in simulation, however, it is necessary to take thorough measurements to ensure the proper functionality. In this way, simulation and measurement can be mutually beneficial to antenna development.

REFERENCES

[1] M. R. Daginnus, A. Stephan, R. P. Kronberger: Simulation and Measurement Results of Complex Integrated Vehicle Antenna Systems for Premium Audio Reception. Society of Automotive Engineers, Inc., 2001

[2] D. T. Paris, W. M. Leach, Jr., and E. B. Joy "Basic Theory of Probe-Compensated Near-Field Measurements," IEEE Trans. Antennas Propagat., Vol. AP-26, No. 3, pp 373-379,. May 1978.

[3] Electromagnetic Software & Systems (EMSS), Stelenbosch, South Africa, "FEKO User's Guide," 1999. URL http://www.feko.co.za

[4] R. M. Barrett and M. H. Barnes, "Automatic Antenna Wavefront Plotter," Electron., vol. 25, pp. 120-125, Jan. 1952.

[5] C. A. Balanis: Antenna Theory. New York, John Wiley & Sons. Inc, 1997.

[6] A. D. Yaghjian, "An Overview of Near-Field Antenna Measurements," IEEE Trans. Antennas Propagat., Vol. AP-34, pp. 30-45, January 1986.

[7] G. J. Burke and A. J. Poggio, "Numerical Electromagnetics Code (NEC) – Part I: Program Description – Theory," Technical Report Lawrence Livermore Laboratory, January 1981.

[8] E. H. Newman, "A User's Manual for the Electromagnetic Surface Patch Code (ESP)," ElectroScience Lab Report 713402-1, Ohio State University, under Grant DAAG29-81-K-0020, for US Army Research Office, Research Triangle Park, NC, 1981.

[9] B. M. Kolundzija, J. S. Ognjanovic, T. K. Sarkar, and R. F. Harrington, "WIPL: A program for Electromagnetic Modeling of Composite-Wire and Plate Structures," IEEE Antennas and Propagation Magazine, 38, 1, February 1996, pp. 75-79.

[10] John F. Shaeffer, "MOM3D Method of Moments Code – Theory Manual," Technical Report, Lockheed Advanced Development Company, March 1992.

[11] D. R. Wilton, S. U. Hwu, "JUNCTION Code User's Manual," Technical Report No. 87-18, Applied Electromagnetics Laboratory, Department of Electrical Engineering, University of Houston, 1987.

[12] D. B. Davison, I. P. Theron, U. Jakobus, F. M. Landstorfer, F. J. C. Meyer, J. Mostert, and J. J. Van Tonder, " Recent Progress on the Anenna Simulation Program FEKO," Proceedings of the 1998 South African Symposium on Communications and Signal Processing, 1998, COMSIG '98, pp 427-430.

[13] J. Perez, F. Saez de Adana, O. Gutierrez, I. Gonzalex, M. F. Catedra, I. Montiel, and J. Guzman, "FASANT: Fast Computer Tool for the Analysis of On-Board Antennas," IEEE Antennas and Propagation Magazine, 41, 2, April 1999, pp 94-98.

[14] J. G. Ferrante and A. Soubeyran, "EMC2000 and its Application to EMC for Components," Proceedings of CemCompo 99, January 1999, pp 85-90.

[15] F. Obelleiro, J. M. Taboada, J. L. Rodriguez, and J. M. Bertolo, "HEMCUVI: A Software Package for the Electromagnetic Analysis and Design of Radiating Systems on Board Real Platforms," IEEE Antennas and Propagation Magazine, 44, 5, October 2002, pp 44-61.

[16] R. F. Harrington, Field Computation by Moment Method, New York, IEEE Press, 1993.

[17] U. Jakobus, F. M. Landstorfer, "Improved PO-MM Hybrid Formulation for Scattering from Three-Dimensional Perfectly Conducting Bodies of Arbitrary Shape," IEEE Transactions on Antennas and Propagation, Vol. 43, NO. 2. February 1993, pp 162-169.

[18] G. A. Thiele, "Overview of selected hybrid methods in radiating system analysis," Proceedings, IEEE, vol. 80, no. 1, pp. 67-78.

[19] S. M. Rao, D. R. Wilton, and A. W. Glisson, "Electromagnetic scattering by surfaces of arbitrary shape," IEEE Transactions on Antennas and Propagation, Vol. AP-30, no. 3, pp. 409-418, May 1982.

[20] L. N. Medgyesi-Mitschang and D. S. Wang, "Hybrid methods for analysis of complex scatters," Proceedings, IEEE, vol. 77, no. 5, pp. 770-779, May 1989.

[21] P. Wertz, V. Cvijic, R. Hoppe, G. Wolfe, and F. M. Landstorfer, "Wave Propagation Modeling Inside Vehicles by Using a Ray Tracing Approach," Institut fur Hochfrequenztechnik, University of Stuttgart, Stuttgart, Germany